protein that might mediate cancer cell-nerve interaction. To confirm overexpression of CD74 in the high perineural invasion group, we analyzed the level of CD74 mRNA by real-time quantitative RT-PCR. The average relative expression level of CD74 (CD74/glyceraldehyde-3-phosphate dehydrogenase) was significantly higher in the high perineural invasion group than in the low perineural invasion group ($P < 0.000005$), although CaPan1 expressed less CD74 than CaPan2 (Fig. 4A). Next, we used an antibody against CD74 to investigate protein expression of CD74 in five pancreatic cancer cell lines. As in the RT-PCR analysis, CaPan2 and CaPan1 showed significantly higher expression of CD74 than the low perineural invasion group (Fig. 4B). Immunocytochemically, CD74 expression in CaPan2 was found on the cell surface and also more intensely in the cytoplasm (Fig. 4C). Immunohistochemical expression of CD74 in mouse s.c. tumors of these cell lines also showed a similar expression pattern and confirmed the usefulness of the CD74 antibody in immunohistochemistry (Fig. 5A).

Immunohistochemical expression of CD74 in pancreatic cancer tissues. To determine whether CD74 is also overexpressed at the protein level in human pancreatic cancer tissues and involved in perineural invasion, we examined CD74 expression in the surgical cases with an immunohistochemical study. Pancreatic ducts in noncancerous tissues of the normal pancreas or chronic pancreatitis were almost negative or focal immunostaining. However, the lymphocytes always stained strongly and thus served as an internal control of positive staining (Fig. 5B). Neural tissue and acinar cells also showed moderate staining focally. Some pancreatic cancer without perineural invasion showed little or moderate CD74 immunoreactivity, whereas pancreatic cancer with perineural invasion tended to show strong CD74 immunoreactivity (Fig. 5C and D). Strong immunoreactivity was generally observed in the cytoplasm (granular or diffuse) and sometime along the cell membranes of cancer cells. We evaluated the relationship between CD74 and clinicopathologic features. Table 2 shows that degree of perineural invasion was significantly associated with CD74 expression ($P < 0.008$). Other clinicopathologic factors were not associated with CD74 expression, although it seemed to decrease with age ($P < 0.025$).

Discussion

Perineural invasion, together with liver metastasis, is one of the poorest prognostic factors after curative resection (22, 23). Many studies on the perineural invasion of pancreatic cancer and other cancers were clinocopathologic studies using surgical specimens or molecular studies associated with neurotrophins (21, 24–28). Recently, *in vitro* models of perineural invasion using prostate cancer cell lines and mouse dorsal nerves were reported and suggested to be useful to investigate the mechanism of perineural invasion *in vitro* (29, 30). In the present study, we successfully established a perineural invasion model *in vivo* for the first time. We transplanted normal human peripheral nerves into NOD/SCID mice because these mice are an excellent tool to establish human tissue–specific metastasis models (31, 32). As expected, nerve tissues were intact even about 100 days after transplantation. In addition, we showed that pancreatic cancer cell lines preserved their ability of perineural invasion to human nerves. Moreover, they had the ability of perineural invasion to mouse s.c. nerve, too. Finally, using a mouse nerve perineural invasion model, we could clearly separate the high and low perineural invasion groups.

To elucidate the characteristic changes associated with perineural invasion, we globally analyzed the gene expression in the high and low perineural invasion groups. Among upgenes, we further investigated the CD74 molecule and

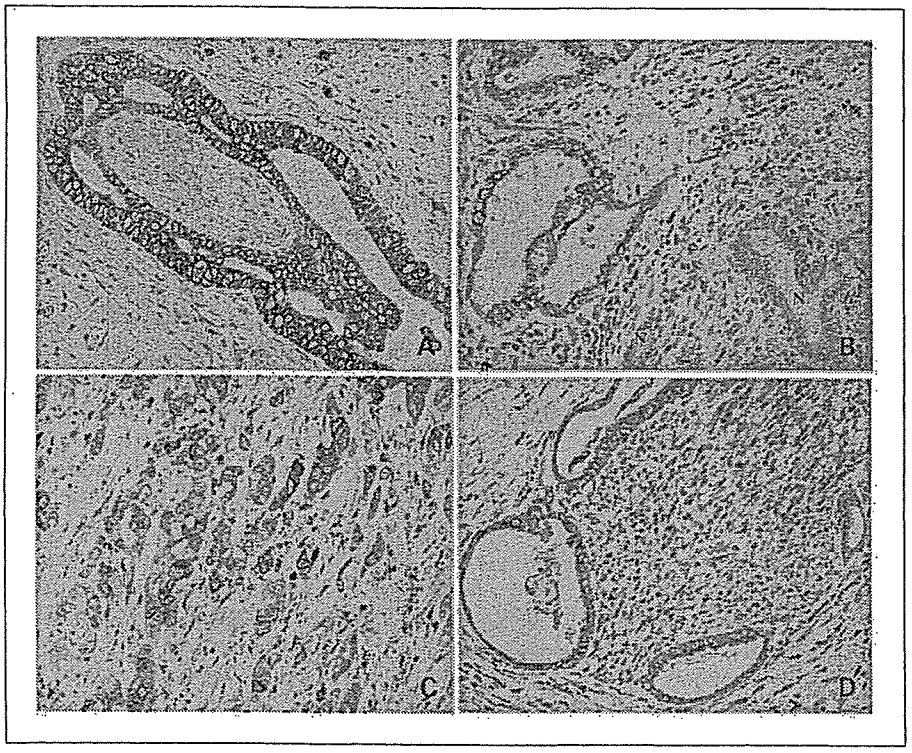

Fig. 5. Immunohistochmical staining of CD74. *A*, CD74 was diffusely expressed in the cytoplasm and cell membrane of CaPan2 demonstrating perineural invasion. *B*, CD74 was negative in the normal pancreatic duct (*N*) but strongly positive in cancer cells and lymphocytes. CD74 was diffusely expressed in poorly differentiated (*C*, perineural invasion 3) and well differentiated (*D*, perineural invasion 3) pancreatic cancer with perineural invasion. Magnification × 200.

Table 2. Immunohistochemical examination of CD74 in human pancreatic cancer tissues

	CD74 expression		P
	−	+	
No. cases	15	52	
Mean age (y)	70.5 ± 9.3	63.9 ± 9.6	0.025
Sex			
Male	10	34	0.9267
Female	5	18	
Differentiation			
Well	7	17	0.499
Intermediate	7	33	
Poor	1	2	
Stroma			
Medullary	0	0	0.622
Intermediate	5	21	
Scirrhous	10	31	
INF			
α	0	0	0.718
β	5	20	
γ	10	32	
Lymphatic invasion			
0-1	11	25	0.073
2-3	4	28	
Lymph node metastasis			
Absent	8	14	0.055
Present	7	38	
Vascular invasion			
0-1	10	24	0.161
2-3	5	28	
Perineural invasion			
0-1	10	15	0.008
2-3	5	37	

confirmed its overexpression in pancreatic cancer and association with perineural invasion. Because two cell lines in high perineural invasion group are better differentiated than three cell lines in low perineural invasion group (33), some of the selected genes might represent tumor differentiation but not perineural invasion. However, it was not likely in case of CD74, because there was no correlation between CD74 expression and tumor differentiation in tumor specimens.

CD74 was originally identified as a γ chain that is associated with the α and β chains of HLA-DR (MHC class II). Many studies have shown that CD74 plays an important role in the assembly, transport, and loading of peptides by HLA-DR molecules. HLA-DR and CD74 interacted in the endoplasmic reticulum immediately after their synthesis. This interaction of CD74 prevented binding by HLA-DR molecules to endogenous peptides (34). This was initially observed on antigen-presenting cells, but recently, it was reported that some malignant cells also expressed CD74, suggesting that CD74 expression might prevent presentation of tumor antigens (35–37). Moreover, preclinical studies in B-cell lymphoma and multiple myeloma showed CD74 was a novel and promising therapeutic target because binding of anti-CD74 monoclonal antibodies became rapidly cointernalized (38–40). Recently, serial analysis of gene expression showed CD74 overexpression in pancreatic cancer (16). In the present study, we confirmed that CD74 was positive in 52 cases (78%) and was overexpressed in cancer cells compared with the pancreatic duct in clinical cases. We suggest that CD74 might also be a novel therapeutic target in pancreatic cancer, especially with perineural invasion.

Although the intracellular portion of CD74 seems to lack a signal-transducing domain, cell proliferation and inhibition of apoptosis through extracellular signal-regulated kinase 1/2 are induced by binding of macrophage migration inhibitory factor (41). Secretion of macrophage migration inhibitory factor is seen in both pancreatitis and pancreatic cancer and induces the production or expression of inflammatory molecules, including IFN-γ (42). IFN-γ also induces further expression of cell surface CD74 (43). Hence, CD74 and these associated molecules might play an important role in the perineural invasion of pancreatic cancer in an autocrine/paracrine manner. Moreover, CD74 has a chondroitin sulfate binding site at the extracellular portion, and this can bind cell surface CD44 (44). CD44 is also expressed in pancreatic cancer and human peripheral nerves. Regarding cancer cell-nerve interaction, interaction of CD74 with CD44 may result in cellular activation and migration and promote perineural invasion.

In addition to CD74, some of the up-regulated genes identified in the present analysis have been recently correlated with tumor growth and invasion in pancreatic cancer. For example, tissue plasminogen activator is a serine protease that catalyses the activation of plasminogen. It is required for cell proliferation and angiogenesis in the early stage of pancreatic cancer (45). γ-Synuclein was initially found in infiltrating breast cancer and was referred to as breast carcinoma-specific gene 1. Overexpression of γ-synuclein protein in pancreatic cancer was correlated with perineural invasion and lymph node metastasis in clinical cases (46).

In conclusion, although the precise mechanism remains to be elucidated, overexpression of CD74 was closely associated with perineural invasion in human pancreatic cancer. We think that this perineural invasion model is the first such report and is an appropriate model for analyzing the mechanism of perineural invasion of human pancreatic cancer.

Acknowledgments

We thank H. Suzuki and Y. Nakamura for technical assistance.

References

1. Jemal A, Murray T, Ward E, et al. Cancer statistics, 2005. CA Cancer J Clin 2005;55:10–30.
2. Parkin DM, Bray FI, Devesa SS. Cancer burden in the year 2000. The global picture. Eur J Cancer 2001;37 Suppl 8:S4–66.
3. Sperti C, Pasquali C, Piccoli A, Pedrazzoli S. Recurrence after resection for ductal adenocarcinoma of the pancreas. World J Surg 1997;21:195–200.
4. Hermanek P. Pathology and biology of pancreatic ductal adenocarcinoma. Langenbecks Arch Surg 1998;383:116–20.
5. Gebhardt C, Meyer W, Reichel M, Wunsch PH. Prognostic factors in the operative treatment of ductal pancreatic carcinoma. Langenbecks Arch Surg 2000; 385:14–20.
6. Amikura K, Kobari M, Matsuno S. The time of occurrence of liver metastasis in carcinoma of the pancreas. Int J Pancreatol 1995;17:139–46.

7. Pour PM, Bell RH, Batra SK. Neural invasion in the staging of pancreatic cancer. Pancreas 2003;26: 322–5.
8. Tsiotos GG, Farnell MB, Sarr MG. Are the results of pancreatectomy for pancreatic cancer improving? World J Surg 1999;23:913–9.
9. Sperti C, Pasquali C, Piccoli A, Pedrazzoli S. Survival after resection for ductal adenocarcinoma of the pancreas. Br J Surg 1996;83:625–31.
10. Bardeesy N, DePinho RA. Pancreatic cancer biology and genetics. Nat Rev Cancer 2002;2:897–909.
11. Crnogorac-Jurcevic T, Efthimiou E, Nielsen T, et al. Expression profiling of microdissected pancreatic adenocarcinomas. Oncogene 2002;21:4587–94.
12. Crnogorac-Jurcevic T, Efthimiou E, Capelli P, et al. Gene expression profiles of pancreatic cancer and stromal desmoplasia. Oncogene 2001;20:7437–46.
13. Han H, Bearss DJ, Browne LW, Calaluce R, Nagle RB, Von Hoff DD. Identification of differentially expressed genes in pancreatic cancer cells using cDNA microarray. Cancer Res 2002;62:2890–6.
14. Iacobuzio-Donahue CA, Maitra A, Shen-Ong GL, et al. Discovery of novel tumor markers of pancreatic cancer using global gene expression technology. Am J Pathol 2002;160:1239–49.
15. Iacobuzio-Donahue CA, Ashfaq R, Maitra A, et al. Highly expressed genes in pancreatic ductal adenocarcinomas: a comprehensive characterization and comparison of the transcription profiles obtained from three major technologies. Cancer Res 2003;63: 8614–22.
16. Hustinx SR, Cao D, Maitra A, et al. Differentially expressed genes in pancreatic ductal adenocarcinomas identified through serial analysis of gene expression. Cancer Biol Ther 2004;3:e19–26.
17. Nomura H, Nishimori H, Yasoshima T, et al. A new liver metastatic and peritoneal dissemination model established from the same human pancreatic cancer cell line: analysis using cDNA macroarray. Clin Exp Metastasis 2002;19:391–9.
18. Sclabas GM, Fujioka S, Schmidt C, et al. Overexpression of tropomysin-related kinase B in metastatic human pancreatic cancer cells. Clin Cancer Res 2005; 11:440–9.
19. Chuma M, Sakamoto M, Yasuda J, et al. Overexpression of cortactin is involved in motility and metastasis of hepatocellular carcinoma. J Hepatol 2004;41:629–36.
20. Japan Pancreas Society. Classification of pancreatic cancer. 2nd English ed. Tokyo: Kanehara; 2003.
21. Kameda K, Shimada H, Ishikawa T, et al. Expression of highly polysialylated neural cell adhesion molecule in pancreatic cancer neural invasive lesion. Cancer Lett 1999;137:201–7.
22. Ishikawa O, Ohigashi H, Sasaki Y, et al. Liver perfusion chemotherapy via both the hepatic artery and portal vein to prevent hepatic metastasis after extended pancreatectomy for adenocarcinoma of the pancreas. Am J Surg 1994;168:361–4.
23. Nitecki SS, Sarr MG, Colby TV, van Heerden JA. Long-term survival after resection for ductal adenocarcinoma of the pancreas. Is it really improving? Ann Surg 1995;221:59–66.
24. Takahashi T, Ishikura H, Motohara T, Okushiba S, Dohke M, Katoh H. Perineural invasion by ductal adenocarcinoma of the pancreas. J Surg Oncol 1997;65: 164–70.
25. Miknyoczki SJ, Lang D, Huang L, Klein-Szanto AJ, Dionne CA, Ruggeri BA. Neurotrophins and Trk receptors in human pancreatic ductal adenocarcinoma: expression patterns and effects on *in vitro* invasive behavior. Int J Cancer 1999;81:417–27.
26. Zhu Z, Friess H, diMola FF, et al. Nerve growth factor expression correlates with perineural invasion and pain in human pancreatic cancer. J Clin Oncol 1999; 17:2419–28.
27. Iwahashi N, Nagasaka T, Tezel G, et al. Expression of glial cell line-derived neurotrophic factor correlates with perineural invasion of bile duct carcinoma. Cancer 2002;94:167–74.
28. Yamaguchi R, Nagino M, Oda K, Kamiya J, Uesaka K, Nimura Y. Perineural invasion has a negative impact on survival of patients with gallbladder carcinoma. Br J Surg 2002;89:1130–6.
29. Ayala GE, Wheeler TM, Shine HD, et al. *In vitro* dorsal root ganglia and human prostate cell line interaction: redefining perineural invasion in prostate cancer. Prostate 2001;49:213–23.
30. Ayala GE, Dai H, Ittmann M, et al. Growth and survival mechanisms associated with perineural invasion in prostate cancer. Cancer Res 2004;64:6082–90.
31. Yonou H, Yokose T, Kamijo T, et al. Establishment of a novel species- and tissue-specific metastasis model of human prostate cancer in humanized non-obese diabetic/severe combined immunodeficient mice engrafted with human adult lung and bone. Cancer Res 2001;61:2177–82.
32. Lock RB, Liem N, Farnsworth ML, et al. The nonobese diabetic/severe combined immunodeficient (NOD/SCID) mouse model of childhood acute lymphoblastic leukemia reveals intrinsic differences in biologic characteristics at diagnosis and relapse. Blood 2002;99:4100–8.
33. Sipos B, Moser S, Kalthoff H, Torok V, Lohr M, Kloppel G. A comprehensive characterization of pancreatic ductal carcinoma cell lines: towards the establishment of an *in vitro* research platform. Virchows Arch 2003;442:444–52.
34. Barrera CA, Almanza RJ, Ogra PL, Reyes VE. The role of the invariant chain in mucosal immunity. Int Arch Allergy Immunol 1998;117:85–93.
35. Hippo Y, Yashiro M, Ishii M, et al. Differential gene expression profiles of scirrhous gastric cancer cells with high metastatic potential to peritoneum or lymph nodes. Cancer Res 2001;61:889–95.
36. Ishigami S, Natsugoe S, Tokuda K, et al. Invariant chain expression in gastric cancer. Cancer Lett 2001; 168:87–91.
37. Jiang Z, Xu M, Savas L, LeClair P, Banner BF. Invariant chain expression in colon neoplasms. Virchows Arch 1999;435:32–6.
38. Burton JD, Ely S, Reddy PK, et al. CD74 is expressed by multiple myeloma and is a promising target for therapy. Clin Cancer Res 2004;10:6606–11.
39. Michel RB, Rosario AV, Andrews PM, Goldenberg DM, Mattes MJ. Therapy of small subcutaneous B-lymphoma xenografts with antibodies conjugated to radionuclides emitting low-energy electrons. Clin Cancer Res 2005;11:777–86.
40. Griffiths GL, Mattes MJ, Stein R, et al. Cure of SCID mice bearing human B-lymphoma xenografts by an anti-CD74 antibody-anthracycline drug conjugate. Clin Cancer Res 2003;9:6567–71.
41. Leng L, Metz CN, Fang Y, et al. MIF signal transduction initiated by binding to CD74. J Exp Med 2003; 197:1467–76.
42. Calandra T, Roger T. Macrophage migration inhibitory factor: a regulator of innate immunity. Nat Rev Immunol 2003;3:791–800.
43. Albanesi C, Cavani A, Girolomoni G. Interferon-gamma-stimulated human keratinocytes express the genes necessary for the production of peptide-loaded MHC class II molecules. J Invest Dermatol 1998;110: 138–42.
44. Naujokas MF, Morin M, Anderson MS, Peterson M, Miller J. The chondroitin sulfate form of invariant chain can enhance stimulation of T cell responses through interaction with CD44. Cell 1993;74:257–68.
45. Diaz VM, Planaguma J, Thomson TM, Reventos J, Paciucci R. Tissue plasminogen activator is required for the growth, invasion, and angiogenesis of pancreatic tumor cells. Gastroenterology 2002;122: 806–19.
46. Li Z, Sclabas GM, Peng B, et al. Overexpression of synuclein-gamma in pancreatic adenocarcinoma. Cancer 2004;101:58–65.

JEM

ARTICLE

Essential roles of DC-derived IL-15 as a mediator of inflammatory responses in vivo

Toshiaki Ohteki,[1] Hiroyuki Tada,[1] Kazuto Ishida,[1] Taku Sato,[1] Chikako Maki,[2] Taketo Yamada,[3] Junji Hamuro,[2] and Shigeo Koyasu[2,4]

[1]Department of Immunology, Akita University School of Medicine, Akita 010-8543, Japan
[2]Department of Microbiology and Immunology and [3]Department of Pathology, Keio University School of Medicine, Tokyo 160-8582, Japan
[4]Core Research for Evolutional Science and Technology, Japan Science and Technology Agency, Kawaguchi 332-0012, Japan

Interleukin (IL)-15 is expressed in a variety of inflammatory diseases. However, the contribution of dendritic cell (DC)–derived IL-15 to the development of diseases is uncertain. Using established models of *Propionibacterium acnes* (*P. acnes*)– and zymosan-induced liver inflammation, we observed granuloma formation in the livers of wild-type (WT) and RAG-$2^{-/-}$ mice but not in those of IL-$15^{-/-}$ mice. We demonstrate that this is likely caused by an impaired sequential induction of IL-12, IFN-γ, and chemokines necessary for monocyte migration. Likewise, lethal endotoxin shock was not induced in *P. acnes*– and zymosan-primed IL-$15^{-/-}$ mice or in WT mice treated with a new IL-15–neutralizing antibody. In both systems, proinflammatory cytokine production was impaired. Surprisingly, neither granuloma formation, lethal endotoxin shock, nor IL-15 production was induced in mice deficient for DCs, and adoptive transfer of WT but not IL-$15^{-/-}$ DCs restored the disease development in IL-$15^{-/-}$ mice. Collectively, these data indicate the importance of DC-derived IL-15 as a mediator of inflammatory responses in vivo.

CORRESPONDENCE
Toshiaki Ohteki:
tohteki@med.akita-u.ac.jp

Abbreviations used: BMDC, BM-derived DC; DAB, 3,3′-diaminobenzidine; DTR, diphtheria toxin receptor; DTR tg, CD11c-DTR-GFP transgenic; GOT and GPT, glutamic-oxaloacetic and -pyruvic transaminase, respectively; GSH, glutathione; H&E, hematoxylin and eosin; HRP, horseradish peroxidase; RA, rheumatoid arthritis.

Proper activation followed by inactivation of immune responses is essential for the maintenance of immunological homeostasis in vivo. Prolonged or aberrant activation of immune responses cause a variety of immunopathological disorders, which often result in tissue destruction mediated by effector cells and cytokines.

We and others have found that IL-15 is a pivotal cytokine for the development and function of innate immune cells, including NK cells, NKT cells, TCR-γδ$^+$ intestinal intraepithelial lymphocytes, and DCs (1–9). IL-15 also affects the acquired immune system because the proliferation and survival of CD8$^+$ T cells with naive and memory phenotypes, as well as antigen-specific memory CD8$^+$ T cells, are impaired in both IL-15Rα$^{-/-}$ and IL-$15^{-/-}$ mice (4, 6, 10–12). These studies showed a beneficial effect of IL-15 on the establishment and maintenance of the immune system against pathogen infections as well as malignancies.

In contrast, circumstantial evidence suggests that IL-15 is also involved in the development of immunopathological disorders. IL-15 mRNA and protein are expressed in synovial membranes in rheumatoid arthritis (RA) (13, 14). It has been suggested that IL-15 precedes TNF-α production in cytokine cascade to recruit T cells into the synovial membranes, possibly contributing to the pathogenesis of RA (13, 14). Supporting this notion, treatment of DBA/1 mice with the soluble IL-15Rα and IL-15 mutant/Fcγ2a fusion protein, which bind the IL-15R with high affinity but do not trigger signaling events, prevents the mice from developing collagen-induced arthritis (15, 16). The elevated numbers of IL-15–expressing cells and/or elevated levels of IL-15 production correlate with the activities of inflammatory bowel disease (17), type C chronic liver disease (18), sarcoidosis (19), and multiple sclerosis (20). These observations suggest a harmful effect of IL-15 in various immunopathological and inflammatory diseases. However, as IL-15 is produced by many cell types, it remains unknown whether development of these diseases attributes to DC-derived IL-15.

In this study we generated new mAbs to detect and block mouse IL-15 activity and established an ELISA system that enabled us to examine the amounts of IL-15 at protein

T. Ohteki and H. Tada contributed equally to this work.
The online version of this article contains supplemental material.

level. Using the mAb and ELISA system combined with gene-targeted mice, we investigated the role of IL-15 in well-characterized inflammatory disease models in mice. We demonstrate that IL-15 is essential for *P. acnes*– and zymosan-induced granuloma formation and subsequent LPS-induced endotoxin shock, as well as liver damage, through induction of proinflammatory cytokines and chemokines. Of interest, the development of liver diseases and endotoxin shock is unaffected in the absence of T, B, and NK cells, whereas it was severely affected in mice lacking DC-derived IL-15. These experiments identify an irreplaceable function of DC-derived IL-15 in bacterial product–mediated inflammatory responses.

RESULTS

Impaired granuloma formation in IL-15$^{-/-}$ mice

P. acnes is suspected to be a causative bacteria for human sarcoidosis, and its cell wall components show strong immunoadjuvant activities, which induce monocyte migration into the liver and granuloma formation (21–23).

To examine the role of IL-15 in the granuloma formation in vivo, control WT and IL-15$^{-/-}$ mice were injected with heat-killed *P. acnes*. Consistent with previous reports (21–23), granuloma formation was evident in the liver of WT mice on day 6 after injection, whereas it was hardly seen in that of IL-15$^{-/-}$ mice (Fig. 1 A, top left and top middle). Importantly, the granuloma formation was substantially restored by IL-15 injection into IL-15$^{-/-}$ mice (Fig. 1 A, top right). It has been reported that on *P. acnes* infection circulating DC precursors migrate into the liver and, in cooperation with Kupffer cells, monocytes, and T cells, participate in the granulomatous reaction (24). Indeed, *P. acnes*–induced granulomas contained CD11c^{+} DCs (Fig. 1 B). The granuloma formation was observed in the liver of RAG-2$^{-/-}$ mice and NK cell–depleted RAG-2$^{-/-}$ mice but was absent in that of IL-15$^{-/-}$RAG-2$^{-/-}$ mice (Fig. 1 A, bottom; and Fig. S1, available at

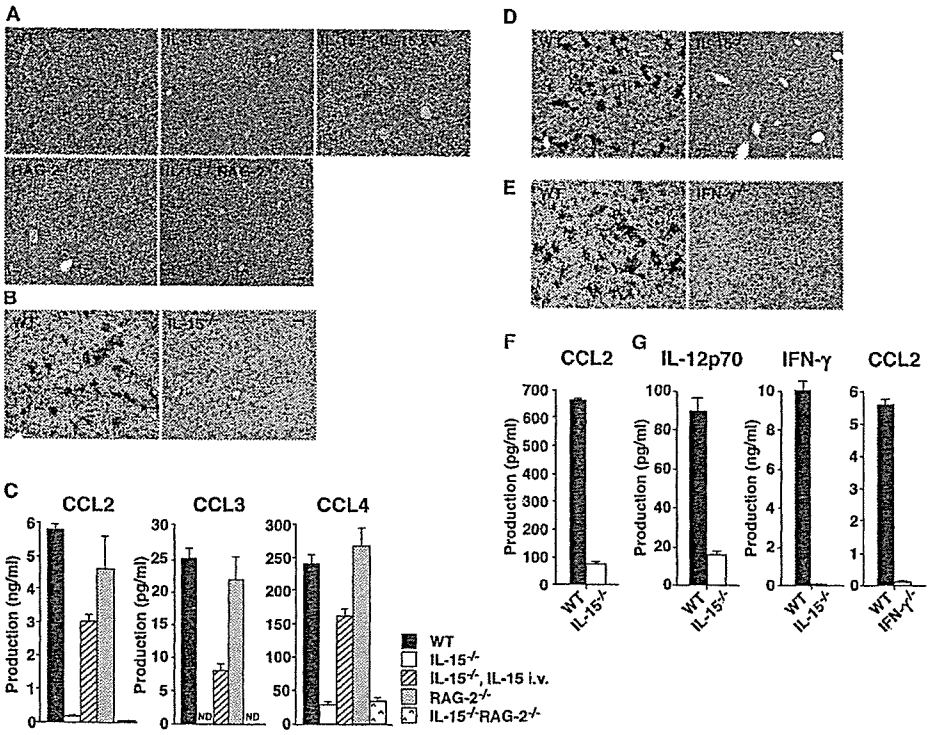

Figure 1. IL-15$^{-/-}$ mice fail to develop *P. acnes*– and zymosan-induced granulomas. (A) Granuloma formation in the liver of WT, IL-15$^{-/-}$, RAG-2$^{-/-}$, and IL-15$^{-/-}$RAG-2$^{-/-}$ mice. Livers were taken on day 6 after a 0.5-mg heat-killed *P. acnes* injection, and sections were stained with H&E. Bar, 100 μm. (B) The liver sections of *P. acnes*-injected WT and IL-15$^{-/-}$ mice were stained with biotinylated anti-CD11c mAb and streptavidin-HRP and further visualized with DAB. Slides were counterstained with Mayer's hematoxylin. Bar, 100 μm. (C) Chemokine levels in the sera of WT, IL-15$^{-/-}$, RAG-2$^{-/-}$, and IL-15$^{-/-}$RAG-2$^{-/-}$ mice were assessed by ELISA at 72 h after a 0.5-mg heat-killed *P. acnes* injection. Values represent SD (n = 3 mice/group). Data are representative of two to four experiments. (D) Granuloma formation in the liver of zymosan-injected WT and IL-15$^{-/-}$ mice. Livers were taken on day 6 after a 1 mg zymosan injection, and sections were stained with biotinylated anti-CD11c mAb and streptavidin-HRP and further visualized with DAB. Slides were counterstained with Mayer's hematoxylin. Bar, 100 μm. (E) The liver sections of *P. acnes*-injected WT and IFN-γ$^{-/-}$ mice were stained as described in B. Bar, 100 μm. (F) 3 d after a 1-mg zymosan injection, CCL2 in the sera of WT and IL-15$^{-/-}$ mice was measured by ELISA. Data are representative of four experiments. (G) 3 d after a 0.5-mg *P. acnes* injection, IL-12p70, and IFN-γ in the sera of WT and IL-15$^{-/-}$ mice and CCL2 in the sera of WT and IFN-γ$^{-/-}$ mice were measured by ELISA. Values represent SD (n = 3 mice/group). Data are representative of three experiments.

http://www.jem.org/cgi/content/full/jem.20061297/DC1), indicating that both T, B, and NK cells are dispensable in the process of granuloma formation. Because chemokine production is critical for monocyte migration into the liver, we next examined the chemokine production, in particular MCP-1 (CCL2) and MIP-1α/β (CCL3/4), which are critical chemoattractants for monocytes. On day 3 after *P. acnes* injection, considerable levels of these chemokines were detected in the sera of WT, RAG-2$^{-/-}$, and NK cell–depleted RAG-2$^{-/-}$ mice (Fig. 1 C and Fig. S2, available at http://www.jem.org/cgi/content/full/jem.20061297/DC1). In contrast, these chemokines were produced only marginally in IL-15$^{-/-}$ and IL-15$^{-/-}$RAG-2$^{-/-}$ mice (Fig. 1 C). Again, the chemokine production was restored by IL-15 injection into IL-15$^{-/-}$ mice. To further examine whether IL-15 directly controls the chemokine production, we analyzed IFN-γ$^{-/-}$ mice. As reported previously (23), *P. acnes*–induced granuloma formation was not seen in the liver of IFN-γ$^{-/-}$ mice (Fig. 1 E). In addition, we found that *P. acnes*–induced IL-12p70 and IFN-γ production in IL-15$^{-/-}$ and CCL2 production in IFN-γ$^{-/-}$ mice was impaired (Fig. 1 G), indicating that IL-15 indirectly induces chemokine production by regulating the IL-12–IFN-γ axis in vivo.

Zymosan is a yeast cell wall particle containing β-glucan and mannan as major components. As *P. acnes* does, zymosan can activate and recruit monocytes, macrophages, and leukocytes (25–27), resulting in the secretion of inflammatory cytokines, hydrogen peroxide, and arachidonic acid (28–30). We also used zymosan to examine the role for IL-15 in the granuloma formation. Consistent with previous experiments (31), zymosan recruited monocytes and DCs and induced granuloma formation in the liver of WT mice. Again, the granulomas were not seen in the liver of IL-15$^{-/-}$ mice (Fig. 1 D), likely because of the lack of chemokine production, such as CCL2 (Fig. 1 F) (31). Our results collectively indicate that IL-15 controls *P. acnes*– and zymosan-induced granuloma formation, likely through the regulation of chemokine production in vivo.

IL-15 regulates LPS-induced lethal endotoxin shock

LPS injection into *P. acnes*–primed mice stimulates DCs and macrophages to produce large amounts of proinflammatory cytokines such as IL-12, IFN-γ, and TNF-α, which cause lethal endotoxin shock in vivo (32–34). Likewise, LPS injection into zymosan-primed mice induces shock and tissue injury (35). We next examined the role of IL-15 in LPS-induced endotoxin shock. On day 6 after a 0.5-mg heat-killed *P. acnes* injection, 1 μg LPS was injected into WT and IL-15$^{-/-}$ mice to induce lethal endotoxin shock. As reported (32–34), *P. acnes*–primed WT mice were sensitive to LPS-induced endotoxin shock, and all mice died within a day. In contrast, IL-15$^{-/-}$ mice were strongly resistant and survived (Fig. 2 A). In addition, NK cell–depleted WT mice, RAG-2$^{-/-}$, mice and NK cell–depleted RAG-2$^{-/-}$ mice died just as control WT mice did, indicating that proinflammatory cytokines produced by T, B, and NK cells are dispensable for the endotoxin shock induction (Fig. 2 A).

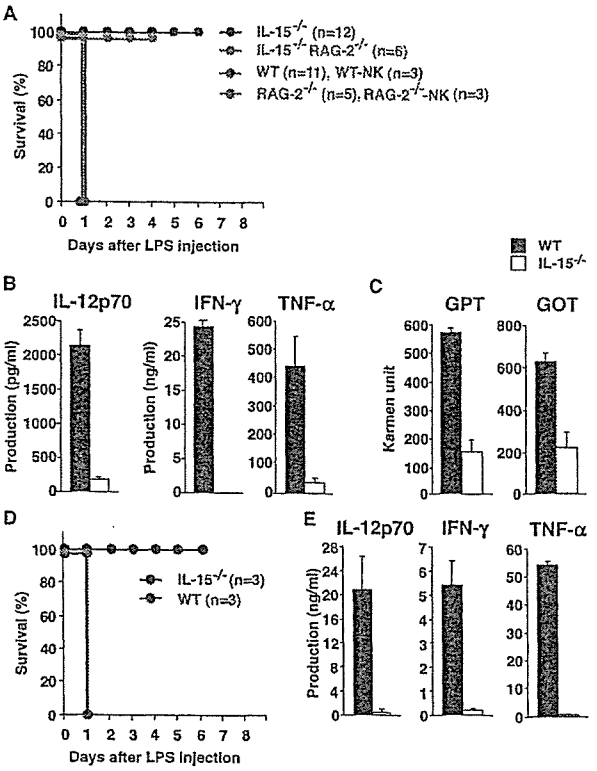

Figure 2. IL-15$^{-/-}$ mice are resistant to LPS-induced lethal endotoxin shock. (A) On day 6 after a 0.5-mg heat-killed *P. acnes* injection, 1 μg LPS were further injected into the indicated mice to induce lethal endotoxin shock. To deplete NK cells, mice were intraperitoneally injected with 300 μg of anti-asialo GM1 polyclonal antibody on the day before and day 3 after *P. acnes* injection. (B) Serum levels of IL-12p70, IFN-γ, and TNF-α were measured by ELISA in *P. acnes*–primed mice at 2 h after LPS injection. Values represent SD (n = 3 WT and 2 IL-15$^{-/-}$ mice/group). Data are representative of three experiments. (C) Serum GOT and GPT levels were assessed in *P. acnes*–primed mice at 2 h after LPS injection. Values represent SD (n = 3 mice/group). Data are representative of two to four experiments. (D) On day 6 after a 1-mg zymosan injection, 10 μg LPS was injected into the indicated mice, and the survival of the mice was monitored. (E) Serum levels of IL-12p70, IFN-γ, and TNF-α were measured by ELISA in zymosan-primed mice at 2 h after LPS injection. Values represent SD (n = 3 mice/group). Data are representative of three experiments.

IL-12, IFN-γ, and TNF-α are known to play important roles in induction of liver injury and/or endotoxin shock (23, 34, 36–39). We thus examined the production of proinflammatory cytokines, in particular IL-12p70, IFN-γ, and TNF-α, in control WT and IL-15$^{-/-}$ mice (Fig. 2 B). Shortly after LPS injection (2 h), these cytokines were detected in the sera of control WT mice, whereas only small amounts of these cytokines were produced in the sera of IL-15$^{-/-}$ mice (Fig. 2 B). Because these cytokines cause liver injury, the level of serum glutamic-pyruvic transaminase (GPT) and glutamic-oxaloacetic transaminase (GOT), an index for hepatocyte damage, was also measured. As expected from the

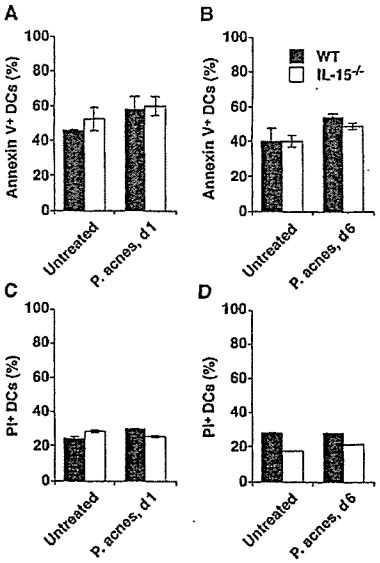

Figure 3. Unaffected apoptosis in IL-15$^{-/-}$ DCs. Splenic DCs were obtained from NK cell-depleted WT and IL-15$^{-/-}$ mice before (untreated) and 1 d (*P. acnes*, d1) and 6 d (*P. acnes*, d6) after heat-killed *P. acnes* injection. (A and B) The proportions of annexin V$^+$ DCs of WT and IL-15$^{-/-}$ mice are shown. (C and D) The proportions of propidium iodide–positive DCs of WT and IL-15$^{-/-}$ mice are shown. Values represent SD ($n = 2$ mice/group). Data are representative of three experiments.

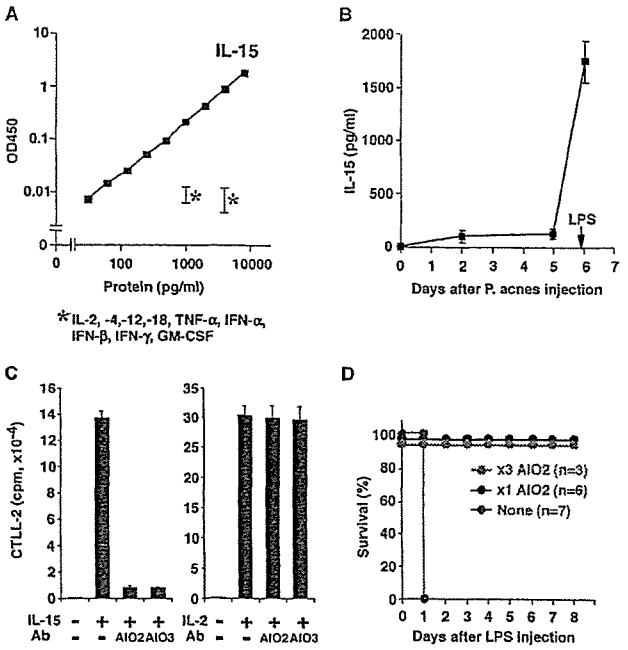

Figure 4. Quantification of IL-15 protein levels by ELISA and treatment of endotoxin shock by IL-15 neutralizing antibody. (A) Newly generated ELISA was specific for mouse IL-15. Specificity of one anti–IL-15 mAb (AIO3) was tested by using the panel of cytokines indicated in the figure. (B) Detection of IL-15 protein in the sera of *P. acnes*– and LPS-injected WT mice. Serum samples were collected from WT and IL-15$^{-/-}$ mice on days 2 and 5 after *P. acnes* injection and at 1.5 h after a subsequent LPS injection on day 6, and levels of IL-15 were assessed with our IL-15 ELISA system. Values represent SD ($n = 3$ mice/group). Data are representative of two to four experiments. (C) To test the capacity of AIO2 and AIO3 to block IL-15 activities, 5×10^4 CTLL-2 cells were stimulated with 10 ng/ml IL-15 or IL-2 in the presence or absence of 10 μg/ml AIO2 or AIO3 for 24 h and pulsed with [^{3}H]thymidine for an additional 8 h. Values represent SD of triplicate cultures. Data are representative of two to four experiments. (D) To examine whether AIO2 can block IL-15 activities in vivo, WT mice were injected with 0.5 mg AIO2 either on day 0, 3, or 6 (x3 AIO2) or only on day 6 (x1 AIO2) after *P. acnes* injection. On day 6, 1 h after AIO2 injection, 1 μg LPS was further injected, and survival of these mice was monitored.

minimal proinflammatory cytokine production, considerable reduction of GPT and GOT release was observed in the sera of IL-15$^{-/-}$ mice, as compared with those in WT mice (Fig. 2 C). Similar to these observations, zymosan-primed IL-15$^{-/-}$ mice exhibited strong resistance to LPS-induced lethality, which was consistent with the reduced production of IL-12, IFN-γ, and TNF-α (Fig. 2, D and E).

Unaffected DC survival in IL-15$^{-/-}$ mice

As recently reported that IL-15 regulates survival of DCs (40), impaired inflammatory responses observed in IL-15$^{-/-}$ mice might be caused by the impaired DC survival. To examine this possibility, we examined the number of splenic DCs between WT and IL-15$^{-/-}$ mice before and after *P. acnes* injection. The numbers of DCs in untreated WT and IL-15$^{-/-}$ mice were $0.83 \times 10^6 \pm 0.15$ ($n = 5$) and $0.82 \times 10^6 \pm 0.13$ ($n = 5$), respectively, and those in *P. acnes*–injected WT and IL-15$^{-/-}$ mice (6 d after injection) were $1.39 \times 10^6 \pm 0.28$ ($n = 4$) and $1.54 \times 10^6 \pm 0.16$ ($n = 4$), respectively. Using annexin V and propidium iodide staining, we further analyzed the number of apoptotic DCs before and after *P. acnes* injection and found no important difference between WT and IL-15$^{-/-}$ DCs (Fig. 3). These results suggested that impaired inflammatory responses observed in IL-15$^{-/-}$ mice are unlikely caused by the impaired DC survival in vivo.

mAb generation to detect and block mouse IL-15 activity

As IL-15 was found to be a critical mediator for granuloma formation and endotoxin shock induction in vivo, it is important to quantitate the amount of IL-15 produced as a soluble protein in mice during the induction phase of granuloma formation and the eliciting phase of endotoxin shock. For this purpose, we generated rat mAbs specific for mouse IL-15 (for details see Materials and methods). Among 108 clones, 2 clones named AIO2 and AIO3 produced mAbs against mouse IL-15, which were suitable as coating antibodies for an ELISA system. Importantly, the newly developed ELISA system is specific for mouse IL-15 and does not cross react with other cytokines tested, which include IL-2, IL-4, IL-12, TNF-α, IFN-α, IFN-β, IFN-γ, and GM-CSF (Fig. 4 A). Using the ELISA system, we found that substantial amounts of IL-15 were produced in the sera of *P. acnes*–injected WT mice, and the IL-15 levels were dramatically enhanced immediately after LPS injection into *P. acnes*–primed WT mice (Fig. 4 B),

which was consistent with the observation that the lack of IL-15 resulted in the impaired endotoxin shock.

The results shown in Fig. 2 (A and D) and Fig. 4 B collectively raised a possibility of treatment of inflammatory diseases by blocking IL-15 activity in vivo. To this end, we examined whether anti–IL-15 mAbs were capable of blocking IL-15 activity (Fig. 4 C). It is well known that both IL-2 and IL-15 efficiently induce proliferation of a T cell line, CTLL-2. As shown in Fig. 4 C, IL-15–dependent proliferation of CTLL-2 was markedly reduced (>95% reduction) in the presence of AIO2 or AIO3, whereas IL-2–dependent proliferation of CTLL-2 was not affected at all by these mAbs, demonstrating that the mAbs efficiently and selectively block IL-15 activity in vitro. We further examined the effect of AIO2 in vivo (Fig. 4 D). WT mice that had been injected with AIO2 on days 0, 3, and 6 after *P. acnes* injection (x3 AIO2) and only on day 6 (1 h before LPS injection, x1 AIO2) were strongly resistant to LPS-induced lethality and survived. The results

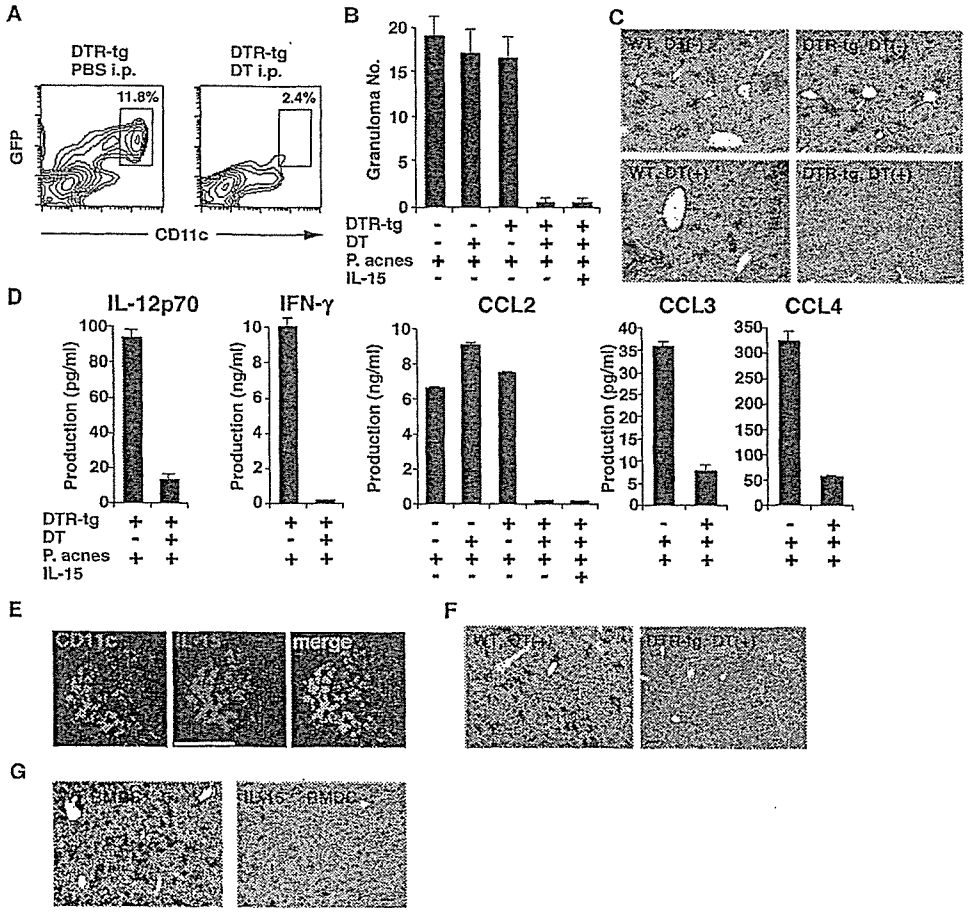

Figure 5. DC-derived IL-15 controls granuloma formation. (A) Spleen cells were obtained from DTR tg mice 24 h after injection of 100 ng DT or PBS and stained with anti-CD11c-PE. The percentages indicate the proportions of DCs in a DC-enriched fraction; i.e., the cells at the interface after a dense BSA gradient centrifugation (see DC preparation... in Materials and methods). (B) Granuloma formation in the liver of *P. acnes*–primed DT-injected DTR tg mice. On day 3 after a 0.5-mg heat-killed *P. acnes* injection, livers were taken from WT and DTR tg mice that had been injected with either PBS or DT on the day before *P. acnes* injection, and sections were stained with H&E. Numbers of granulomas were counted in five different fields under a microscope. Values represent SD (n = 3 mice/group). Data are representative of three experiments. (C) To test whether DCs were present in the granuloma regions, the liver sections were stained with biotinylated anti-CD11c mAb and streptavidin-HRP and further visualized with DAB. Slides were counterstained with Mayer's hematoxylin. Bar, 100 μm. (D) IL-12p70, IFN-γ, and chemokine levels in the sera of DT-injected DTR tg mice were assessed by ELISA at 72 h after a 0.5-mg heat-killed *P. acnes* injection. Values represent SD (n = 3 mice/group). Data are representative of three experiments. (E) Immunofluoresence staining for the identification of IL-15–producing cells. Acetone-fixed frozen tissue sections were incubated with FITC-conjugated anti-CD11c (clone N418) and biotinylated anti–IL-15 antibodies and further developed with streptavidin-PE. Bar, 50 μm. (F) Granuloma formation in the liver of zymosan-primed DT-injected DTR tg mice. As described in B and C, livers were taken from the indicated mice on day 3 after a 1-mg zymosan injection, and sections were stained for CD11c. Slides were counterstained with Mayer's hematoxylin. Bar, 100 μm. (G) Granuloma formation in the liver of BMDC-injected IL-15$^{-/-}$ mice. IL-15$^{-/-}$ mice were injected with 1 × 10^6 WT BMDCs or IL-15$^{-/-}$ BMDCs. After 12 h, mice were injected with 0.5 mg *P. acnes*, and granuloma formation was analyzed 6 d later as described in B, C, and F. Bar, 100 μm.

clearly show that antibody capable of neutralizing IL-15 activity is effective in blocking endotoxin shock in vivo.

Essential roles for DC-derived IL-15 in inflammatory response induction

As DCs are present in granuloma regions (Fig. 1, B, D, and E), we further examined the role of DCs in the granuloma formation using CD11c–diphtheria toxin receptor (DTR)–GFP transgenic (DTR tg) mice (41). Because the mice carry a transgene encoding DTR-GFP fusion protein under the control of a mouse CD11c promoter, DT injection induces selective depletion of DCs in vivo (Fig. 5 A) (41). *P. acnes*– and zymosan-induced (Fig. 5, B and C; and Fig. 5 F, respectively) granulomas were observed in the livers of untreated WT, DT-injected WT, and untreated DTR tg mice, as expected. In contrast, neither $CD11c^+$ DCs nor granulomas themselves were observed in the DT-injected DTR tg mice (Fig. 5, B, C, and F). Consistent with this observation, production of IL-12p70, IFN-γ, CCL2, and CCL3/4 was impaired in the DT-injected DTR tg mice, as observed in $IL\text{-}15^{-/-}$ mice (Fig. 5 D). Importantly, immunohistochemical analysis revealed that many IL-15–producing cells in granuloma regions were $CD11c^+$ DCs (Fig. 5 E). Contrary to the case of $IL\text{-}15^{-/-}$ mice, however, IL-15 administration restored neither the *P. acnes*–induced granulomatous liver disease nor CCL2 production in DC-depleted DTR tg mice (Fig. 5, B and D), implying that direct action of DC-derived IL-15 on DCs is necessary for the chemokine-mediated granuloma formation in vivo. To formally demonstrate the importance of DC-derived IL-15 in the granuloma formation, BM-derived DCs (BMDCs) of WT and $IL\text{-}15^{-/-}$ mice were adoptively transferred into $IL\text{-}15^{-/-}$ mice. Importantly, the granuloma formation was substantially restored by the injection of WT but not $IL\text{-}15^{-/-}$ BMDCs into $IL\text{-}15^{-/-}$ mice (Fig. 5 G), demonstrating that DC-derived IL-15 is essential for the granuloma formation.

Intracellular redox status affects the pattern of cytokine production by DCs and macrophages (42–45). For example, reductive DCs (and macrophages) with elevated intracellular glutathione (GSH) preferentially produce IL-12 and are involved in Th1 responses, whereas oxidative DCs with reduced GSH produce IL-10 and PGE_2, which lead to Th2 cell induction. As *P. acnes* priming efficiently induces reductive status in DCs (44), we next examined the role for IL-15 in determining redox status in DCs (Fig. S3, available at http://jem.org.cgi/content/full/jem.20061297/DC1). As previously shown (44), *P. acnes* injection clearly induced a reductive condition with elevated intracellular GSH levels in WT DCs. In contrast, such a reductive condition was not induced, if any, in $IL\text{-}15^{-/-}$ DCs on *P. acnes* stimulation. These data indicate that IL-15 is one of the critical cytokines in reductive DC differentiation.

We also examined the role of DCs in endotoxin shock. 1 d after DT injection, control WT and DTR tg mice were primed with 0.5 mg *P. acnes*. On day 3 after *P. acnes* injection, these mice were injected with 1 μg LPS, and survival rate was monitored. On LPS injection, all *P. acnes*–primed WT and DT-untreated DTR tg mice died of endotoxin shock within 24 h (Fig. 6 A). However, *P. acnes*–primed and DT-injected DTR tg mice survived much longer than control mice, indicating that DCs play a pivotal role in endotoxin shock as well. Of note, DT-injected DTR tg mice survived relatively shorter than $IL\text{-}15^{-/-}$ mice (Fig. 2 A), which was likely because of the gradual recovery of DCs in DT-injected DTR tg mice as reported previously (41). *P. acnes*–primed DT-injected DTR tg mice showed impaired production of IL-15 and IL-15–regulated proinflammatory cytokines, IL-12p70, IFN-γ, and TNF-α on LPS stimulation (Fig. 6 B). In addition, WT BMDC-transferred $IL\text{-}15^{-/-}$ mice became sensitive to the endotoxin shock, and all mice died within a day, whereas $IL\text{-}15^{-/-}$ BMDC–injected $IL\text{-}15^{-/-}$ mice remained resistant (Fig. 6 C). Collectively, these results indicate that DC-derived IL-15 is critical for endotoxin shock induction in vivo.

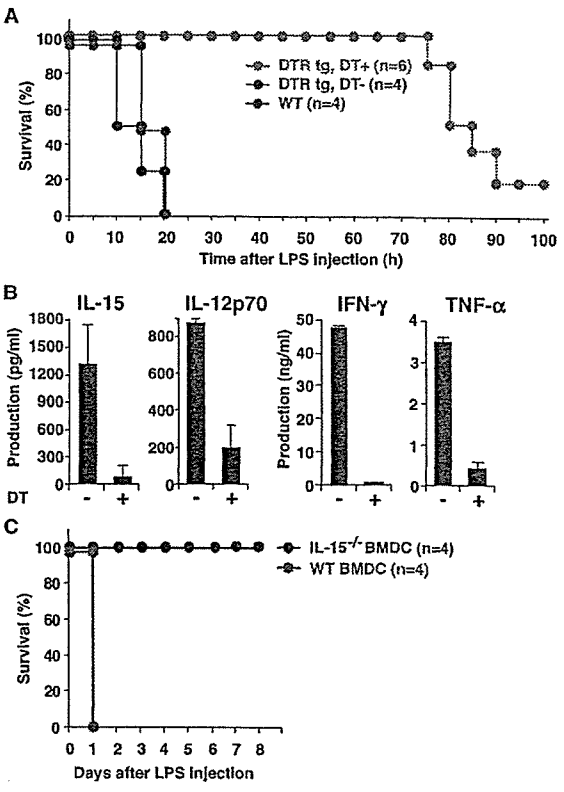

Figure 6. DC-derived IL-15 regulates endotoxin shock. (A) 1 d after DT injection, control WT and DTR tg mice were primed with 0.5 mg *P. acnes*. On day 3 after *P. acnes* injection, these mice were further injected with 1 μg LPS, and survival rate was monitored. (B) Serum levels of IL-15, IL-12p70, IFN-γ, and TNF-α were assessed in DT-injected and *P. acnes*–primed DTR tg mice at 2 h after LPS injection. Values represent SD ($n = 3$ mice/group). Data are representative of three experiments. (C) $IL\text{-}15^{-/-}$ mice were injected with 1×10^6 WT or $IL\text{-}15^{-/-}$ BMDCs. After 12 h, mice were injected with 0.5 mg *P. acnes*. On day 6 after *P. acnes* injection, these mice were further injected with 5 μg LPS, and survival rate was monitored.

DISCUSSION

DC-derived IL-15

Prolonged or aberrant activation of immune responses cause a variety of immunopathological disorders that are often mediated by effector cells and cytokines. We previously found that DC-derived IL-15 is required for the functional maturation of DCs, such as IL-12 production in response to LPS and agonistic anti-CD40 mAb combined with IL-4 stimulation in vitro (8), and have recently shown that DC-derived IL-15 is essential for CpG-induced protective immune activation against pathogen infections in vivo (9). In contrast to the beneficial effect of DC-derived IL-15, we maintain in this study that DC-derived IL-15 has harmful aspects and causes inflammatory diseases, such as granuloma formation and endotoxin shock in vivo.

IL-15 is involved in a variety of inflammatory and autoimmune diseases (13, 14, 17–20). To address whether development of these diseases attributes to IL-15, analyses using IL-15$^{-/-}$ mice, anti–IL-15 neutralizing antibody, soluble IL-15Rα, and IL-15 mutant/Fcγ2a fusion protein are in progress in both human and mouse models (15, 16). As IL-15 is produced by multiple cell types, which include DCs, macrophages, monocytes, and endothelial cells (5), an advanced and unresolved question has been whether DC-derived IL-15 is exclusively required for the development of certain diseases in vivo. Numerous previous in vitro studies indicated that DC-derived IL-15 is capable of inducing activation of Th1 cells, CTL, NK cells, monocyte differentiation into DCs, and antigen-processing machinery in DCs (5, 46), but these studies did not directly prove the irreplaceable role of DC-derived IL-15 in disease development in vivo, where multiple IL-15 producers are present. To address this issue, it is important to show that the development of certain diseases is impaired in IL-15$^{-/-}$ or WT mice treated with reagents to block IL-15 activity, and to further restore the disease development by adoptively transferring WT but not IL-15$^{-/-}$ DCs into these mice. In this respect, only one paper has shown that IL-15$^{-/-}$ or WT mice treated with soluble IL-15Rα were impaired in CD8^{+} T cell–dependent delayed-type hypersensitivity response, and the delayed-type hypersensitivity response was restored by injecting antigen-labeled WT DCs in vivo (47). It is unclear, however, whether IL-15 is important for cytokine production or antigen presentation in this study (47). Other groups have shown that IL-15Rα and IL-15 expression by hematopoietic cells is critical for the maintenance of antigen-specific memory CD8^{+} T cells and bystander CD8^{+} T cell proliferation through a "transpresentation" pathway (48–53), and implied DCs as the major source of IL-15 but never proved it. Accordingly, it remains unknown whether DC-derived IL-15 is essential in the maintenance of innate and acquired immune responses, and whether it causes inflammatory disease development in vivo. It is thus important to prove the in vivo role of DC-derived IL-15 for the development of antiinflammatory drugs that selectively block the DC-derived IL-15 activity.

Mechanisms of how IL-15 controls cytokine production are unknown. As shown in this paper, IL-15 increased the intracellular GSH levels in DCs. Intracellular GSH levels in DCs and macrophages play an important role in determining the profiles of proinflammatory cytokines (42–45). We have previously demonstrated that reductive DCs with high intracellular GSH levels preferentially produce IFN-γ, which in turn augment GSH levels in the cells (44). As shown in this paper, IL-15 is also one of the positive regulators of intracellular GSH status in DCs, augmenting the production of proinflammatory cytokines. In future studies, it should be determined how IL-15 controls the amounts of intracellular GSH in DCs.

Granuloma formation, liver injury, and IL-15

The number of *P. acnes*–induced granulomas and LPS-induced hepatic necrosis after priming with *P. acnes* are substantially reduced in IFN-γ$^{-/-}$ mice (Fig. 1 E) (23). In addition, *P. acnes* does not induce granuloma formation in TNF-RI$^{-/-}$ mice and mice treated with soluble TNF-RI (21). These studies clearly demonstrate the importance of IFN-γ and TNF-α in *P. acnes*–induced liver diseases in vivo. In contrast, it has been shown that CCL3 attracts DC precursors in the blood into the sinusoidal granuloma and lets them participate in inflammatory responses in *P. acnes*–primed mice (24). In addition, CCL2 has also been reported as an important monocyte chemoattractant for granuloma models induced by zymosan, *P. acnes*, and *Mycobacterium tuberculosis* (54–56). These studies show that the chemokines play a critical role in granuloma models, though the importance of IFN-γ and TNF-α in chemokine production remains unclear. Notably, we determined that an IL-15–IL-12–IFN-γ–chemokine (CCL2/3/4) axis in innate immune system is essential, whereas T and B cells are dispensable for the development of granulomatous disease and/or liver injury. Immunohistochemical analysis revealed that DCs preferentially expressed IL-15 in the granuloma regions, and the granuloma formation was impaired in mice lacking DC and DC-derived IL-15 production, clearly demonstrating that DC-derived IL-15 is an initiator for the development of liver diseases.

Of note, IL-15 injection restored the granuloma formation in the liver of IL-15$^{-/-}$ mice but not DC-depleted DTR tg mice. These results suggest that a critical first step for the granuloma formation is to stimulate DCs with DC-derived IL-15 in an autocrine manner. Although Kupffer cells are critically involved as initial antigen-presenting (*P. acnes* and zymosan) cells (24), Kupffer cells isolated from *P. acnes*–primed mice were unable to produce IL-15 on LPS stimulation in vitro (unpublished data).

Endotoxin shock and IL-15

LPS-induced liver injury is closely coupled to endotoxin shock. Indeed, mice deficient in IL-12, IFN-γ, TNF-α, or the receptors for these cytokines displayed resistance to LPS-induced endotoxin shock (34, 36, 38, 57). We showed in this paper that DCs are essential for endotoxin shock, and

DC-derived IL-15 controls endotoxin shock induction by controlling the production of IL-12, IFN-γ, and TNF-α, as DC-depleted mice produced these cytokines at much reduced levels, and WT DC-injected IL-15$^{-/-}$ mice became sensitive to endotoxin shock. Contrary to IL-15$^{-/-}$ mice, *P. acnes*–primed IL-18$^{-/-}$ mice showed much higher TNF-α production and susceptibility to LPS-induced endotoxin shock (58). Together with our results, IL-15 and IL-18 function apparently through distinct pathways in terms of TNF-α production, and IL-15 induces, whereas IL-18 suppresses, TNF-α production.

Collectively, we propose here that DC-derived IL-15 is a master regulator of inflammatory responses in granulomatous liver diseases and related endotoxin shock. Indeed, DC-derived IL-15 regulates the production of IL-12p70, IFN-γ, TNF-α, and downstream CCL2/3/4. Given that elevated IL-15 production and IL-15–expressing cells are evident in RA (13, 14), inflammatory bowel disease (17), type C chronic liver disease (18), sarcoidosis (19), multiple sclerosis (20), and celiac disease (59), it is important to further investigate the roles of IL-15 in these inflammatory diseases and search for the propriety of IL-15 as a target for the development of antiinflammatory drugs.

MATERIALS AND METHODS

Mice. B6–IL-15$^{-/-}$ (IL-15$^{-/-}$) mice (6) were purchased from Taconic, and B6-RAG2$^{-/-}$ (RAG2$^{-/-}$) mice were provided by Taconic and Central Laboratories for Experimental Animals. B6–IFN-γ$^{-/-}$ mice were purchased from The Jackson Laboratory. To obtain B6–IL-15$^{-/-}$RAG2$^{-/-}$ mice (IL-15$^{-/-}$ × RAG2$^{-/-}$), F_1 mice were backcrossed with RAG2$^{-/-}$ mice, and the obtained IL-15$^{+/-}$RAG2$^{-/-}$ mice were intercrossed. The offspring were genotyped for IL-15, and IL-15$^{-/-}$RAG2$^{-/-}$ mice were used for experiments. B6-CD11c-DTR-GFP mice (41) were provided by Steffen Jung, Dan R. Littman, and Richard A. Lang (New York University School of Medicine, New York, NY). All mice were maintained in our specific pathogen-free animal facility, and experiments were performed between 6–12 wk of age in accordance with the guidelines of the Institutional Animal Care Committee of Akita University and Keio University School of Medicine.

Histologic and immunohistochemical analysis. Frozen livers embedded in OCT compound (Sakura Finetek) were sliced into 5-μm-thick sections and fixed with 1% paraformaldehyde and stained with Mayer's hematoxylin and eosin (H&E). Sections of livers were observed with a microscope (DM4500 B; Leica). For CD11c immunostaining, acetone-fixed 5-μm fresh-frozen tissue sections were incubated with biotinylated anti-CD11c mAb (clone, N418; eBioscience) overnight at 4°C and with streptavidin-conjugated horseradish peroxidase (HRP; PerkinElmer). Sections were immunostained using 3,3′-diaminobenzidine (DAB) substrate liquid (DakoCytomation). Slides were counterstained with Mayer's hematoxylin. For CD11c and IL-15 double immunofluorescence staining, acetone-fixed 5-μm fresh-frozen tissue sections were incubated with FITC-conjugated anti-CD11c (clone, N418; eBioscience) and biotinylated goat anti–mouse IL-15 polyclonal antibody (R&D Systems) for 1 h at room temperature. Sections were further stained with streptavidin-conjugated PE (eBioscience) for 30 min at room temperature and observed by fluorescence microscopy.

Measurement of serum chemokines, cytokines, GPT, and GOT. Levels of IL-12p70, IFN-γ, TNF-α, and CCL2/3/4 in the sera were measured by ELISA kits (IL-12p70, IFN-γ, and TNF-α were obtained from BD Biosciences; CCL2/3/4 was obtained from R&D Systems), according to the manufacturer's instructions. The concentrations of cytokines were determined using a data analysis program (Softmax PRO; Molecular Devices). Serum GPT and GOT levels were determined with Fuji Dri-Chem 5500V (Fuji Medical System), according to the manufacturer's instructions.

Generation of anti–mouse IL-15 mAb and ELISA for mouse IL-15. To detect mouse IL-15 protein, mAbs specific for mouse IL-15 were generated by immunizing mouse IL-15 into Lewis rat. Using conventional methods, spleen cells isolated from the immunized rat were fused with X63-Ag8.653 myeloma cells, and limiting dilution for hybridoma cells was performed. Positive clones producing anti–IL-15 mAb were screened based on the binding capacity to coated mouse IL-15. Among the mAbs, AIO2 and AIO3 clones were further selected as neutralizing mAbs based on the inhibition of IL-15–dependent CTLL-2 cell proliferation. In brief, 5 × 10^4 CTLL-2 cells were cultured with 10 ng/ml IL-15 or IL-2 in the presence or absence of 10 μg/ml AIO2 and AIO3 for 24 h and pulsed with [^{3}H]thymidine for an additional 8 h. For mouse IL-15 sandwich ELISA, microwells were coated with AIO3 overnight at 4°C and incubated with Block Ace (Dainippon Pharmaceutical) for 90 min. The diluted serum samples were incubated for 2 h, then for 60 min with biotinylated goat anti–mouse IL-15 antibody (R&D Systems) and for 60 min with avidin-HRP (Sigma-Aldrich). The absorbance of substance released from the substrate was measured at 450 nm. The IL-15 concentrations in samples were determined using Softmax PRO, based on a standard curve of recombinant mouse IL-15.

Reagents and in vivo treatment. Mice were injected with either 0.5 mg of heat-killed *P. acnes* (American Type Culture Collection) or 1 mg of zymosan (Sigma-Aldrich). 6 d later, the amounts of LPS indicated in the figures (*Escherichia coli* O55:B5; Sigma-Aldrich) were further injected into *P. acnes*– and zymosan-primed mice, respectively, to induce endotoxin shock. To deplete NK cells, 300 μg/200 μl of polyclonal anti-asialo GM1 (Wako) was injected. To neutralize IL-15 in vivo, 0.5 mg AIO2 was injected. For systemic DC depletion in vivo, CD11c-DTR-GFP mice were injected intraperitoneally with 100 ng/body of diphtheria toxin (Sigma-Aldrich).

DC preparation, detection of apoptosis, and adoptive transfer. DCs were prepared from spleens as previously described (8). In brief, collagenase-digested spleen cells were suspended in a 28% BSA solution in 1.08 g/ml PBS, overlaid with 1 ml FCS-free RPMI 1640 medium (Sigma-Aldrich), and centrifuged at 9,500 *g* for 20 min at 4°C. The cells at the interface were collected, washed, and resuspended. DCs were further purified using anti-CD11c (clone N418) microbeads with an autoMACS separation system (Miltenyi Biotec). To detect apoptotic DCs, 5 × 10^5 DCs were cultured in vitro for 6 h and incubated for 15 min at room temperature in 500 μl annexin V binding buffer with 150 ng/ml annexin V (R&D Systems) or for 10 min at 4°C in 500 μl PBS with 2 μg/ml propidium idodide (Sigma-Aldrich), respectively. For generation of BMDCs, WT and IL-15$^{-/-}$ BM cells were cultured at 1.5 × 10^6 cells/ml in 10% FCS RPMI 1640 medium in the presence of 10 ng/ml GM-CSF (RDI Division of Fitzgerald Industries). After 3 d of culture, half of the medium was exchanged with a fresh one. After 6 d of culture, BMDCs were purified using anti-CD11c microbeads with an autoMACS separation system. For adoptive transfer experiments, 1 × 10^6 BMDCs were intravenously injected into IL-15$^{-/-}$ mice.

Qualitative determination of intracellular GSH with ACAS. The procedures have previously been described (44). In brief, 300 μl of a suspension of splenic DCs, adjusted to a density of 3 × 10^5 cells/ml in an RPMI 1640 (phenol red free) medium, were applied into a chamber slide (Lab-Tek; Nunc) and incubated for 3 h. After washing, 300 μl of 10 μM monochlorobiman was added, and the reaction was conducted for 30 min. The fluorescence intensity was monitored by argon-ion laser cytometry with a workstation (ACAS 570; Meridian Instruments). Intracellular GSH levels were detected with an excitation wavelength of 350 nm and an emission wavelength of 460 nm.

Online supplemental material. Fig. S1 shows granuloma formation in the liver of NK cell–depleted RAG-2$^{-/-}$ mice. Fig. S2 shows the level of

serum CCL2 in NK cell–depleted RAG-2$^{-/-}$ mice. Fig. S3 shows reductive status in *P. acnes*–stimulated IL-15$^{-/-}$ DCs.

We thank M. Shibata, N. Kakizaki, and M. Motouchi for animal care; M. Kondo and K. Maekawa for screening of hybridoma cells and mAb purification; K. Yamashita and Y. Abe for experimental support; and T. Yoshimoto and K. Nakanishi for Kupffer cell isolation and critical reading of the manuscript.

This work was supported in part by the Toray Science Foundation (T.Ohteki); the Uehara Memorial Foundation (T.Ohteki); the Takeda Science Foundation (T. Ohteki); the Novartis Foundation for the Promotion of Science (T. Ohteki); the Sankyo Foundation for Life Science (T. Ohteki); grants-in-aid for Scientific Research on Priority Areas from the Ministry of Education, Culture, Sports, Science and Technology of Japan (14021110 to S. Koyasu; 16017212 and 16043204 to T. Ohteki); the 21st Century Center of Excellence Program; a Keio University special grant-in-aid for Innovative Collaborative Research Projects; and the Uehara Memorial Foundation special project research grant (to S. Koyasu). H. Tada is supported by a research fellowship from the Japan Society for the Promotion of Science for Young Scientists.

The authors have no conflicting financial interests.

Submitted: 19 June 2006
Accepted: 14 August 2006

REFERENCES

1. Ohteki, T., S. Ho, H. Suzuki, T.W. Mak, and P.S. Ohashi. 1997. Role for IL-15/IL-15 receptor β-chain in natural killer 1.1$^+$ T cell receptor-αβ$^+$ cell development. *J. Immunol.* 159:5931–5935.
2. Ogasawara, K., S. Hida, N. Azimi, Y. Tagaya, T. Sato, T. Yokochi-Fukada, T.A. Waldmann, T. Taniguchi, and S. Taki. 1998. Requirement for IRF-1 in the microenvironment supporting development of natural killer cells. *Nature.* 391:700–703.
3. Ohteki, T., H. Yoshida, T. Matsuyama, G.S. Duncan, T.W. Mak, and P.S. Ohashi. 1998. The transcription factor interferon regulatory factor 1 (IRF-1) is important during the maturation of natural killer 1.1$^+$ T cell receptor-α/β$^+$ (NK1$^+$ T) cells, natural killer cells, and intestinal intraepithelial T cells. *J. Exp. Med.* 187:967–972.
4. Lodolce, J.P., D.L. Boone, S. Chai, R.E. Swain, T. Dassopoulos, S. Trettin, and A. Ma. 1998. IL-15 receptor maintains lymphoid homeostasis by supporting lymphocyte homing and proliferation. *Immunity.* 9:669–676.
5. Waldmann, T.A., and Y. Tagaya. 1999. The multifaceted regulation of interleukin-15 expression and the role of this cytokine in NK cell differentiation and host response to intracellular pathogens. *Annu. Rev. Immunol.* 17:19–49.
6. Kennedy, M.K., M. Glaccum, S.N. Brown, E.A. Butz, J.L. Viney, M. Embers, N. Matsuki, K. Charrier, L. Sedger, C.R. Willis, et al. 2000. Reversible defects in natural killer and memory CD8 T cell lineages in interleukin 15–deficient mice. *J. Exp. Med.* 191:771–780.
7. Mattei, F., G. Schiavoni, F. Belardelli, and D.F. Tough. 2001. IL-15 is expressed by dendritic cells in response to type I IFN, double-stranded RNA, or lipopolysaccharide and promotes dendritic cell activation. *J. Immunol.* 167:1179–1187.
8. Ohteki, T., K. Suzue, C. Maki, T. Ota, and S. Koyasu. 2001. Critical role of IL-15–IL-15R for antigen-presenting cell functions in the innate immune response. *Nat. Immunol.* 2:1138–1143.
9. Kuwajima, S., T. Sato, K. Ishida, H. Tada, H. Tezuka, and T. Ohteki. 2006. Interleukin 15-dependent crosstalk between conventional and plasmacytoid dendritic cells is essential for CpG-induced immune activation. *Nat. Immunol.* 7:740–746.
10. Becker, T.C., E.J. Wherry, D. Boone, K. Murali-Krishna, R. Antia, A. Ma, and R. Ahmed. 2002. Interleukin 15 is required for proliferative renewal of virus-specific memory CD8 T cells. *J. Exp. Med.* 195:1541–1548.
11. Goldrath, A.W., P.V. Sivalumar, M. Glaccum, M.K. Kennedy, M.J. Bevan, C. Benoist, D. Mathis, and E.A. Butz. 2002. Cytokine requirements for acute and basal homeostatic proliferation of naive and memory CD8$^+$ T cells. *J. Exp. Med.* 195:1515–1522.
12. Schluns, K.S., K. Williams, A. Ma, X.X. Zheng, and L. Lefrançois. 2002. Requirement for IL-15 in the generation of primary and memory antigen-specific CD8 T cells. *J. Immunol.* 168:4827–4831.
13. McInnes, I.B., J. Al-Mughales, M. Field, B.P. Leung, F.-P. Huang, R. Dixon, R.D. Sturrock, P.C. Wilkinson, and F.Y. Liew. 1996. The role of interleukin 15 in T-cell migration and activation in rheumatoid arthritis. *Nat. Med.* 2:175–182.
14. McInnes, I.B., B.P. Leung, R.D. Sturrock, M. Field, and F.Y. Liew. 1997. Interleukin-15 mediates T cell-dependent regulation of tumor necrosis factor-α production in rheumatoid arthritis. *Nat. Med.* 3:189–195.
15. Ruchatz, H., B.P. Leung, X. Wei, I.B. McInnes, and F.Y. Liew. 1998. Soluble IL-15 receptor α-chain administration prevents murine collagen-induced arthritis: a role for IL-15 in development of antigen-induced immunopathology. *J. Immunol.* 160:5654–5660.
16. Ferrari-Lacraz, S., E. Zanelli, M. Neuberg, E. Donskoy, Y.S. Kim, X.X. Zheng, W.W. Hancock, W. Maslinski, X.C. Li, T.B. Strom, and T. Moll. 2004. Targeting IL-15 receptor-bearing cells with an antagonist mutant IL-15/Fc protein prevents disease development and progression in murine collagen-induced arthritis. *J. Immunol.* 173:5818–5826.
17. Kirman, I., and O.H. Nielsen. 1996. Increased numbers of interleukin-15-expressing cells in active ulcerative colitis. *Am. J. Gastroenterol.* 91: 1789–1794.
18. Kakumu, S., A. Okumura, T. Ishikawa, M. Yano, A. Enomoto, H. Nishimura, K. Yoshioka, and Y. Yoshikai. 1997. Serum levels of IL-10, IL-15 and soluble tumour necrosis factor-alpha (TNF-α) receptors in type C chronic liver disease. *Clin. Exp. Immunol.* 109:458–463.
19. Agostini, C., L. Trentin, M. Facco, R. Sancetta, A. Cerutti, C. Tassinari, L. Cimarosto, F. Adami, A. Cipriani, R. Zambello, and G. Semenzato. 1996. Role of IL-15, IL-2 and their receptors in the development of T cell alveolitis in pulmonary sarcoidosis. *J. Immunol.* 157:910–918.
20. Kivisäkk, P., D. Matusevicius, B. He, M. Söderström, S. Fredrikson, and H. Link. 1998. IL-15 mRNA expression is up-regulated in blood and cerebrospinal fluid mononuclear cells in multiple sclerosis (MS). *Clin. Exp. Immunol.* 111:193–197.
21. Senaldi, G., S. Yin, C.L. Shaklee, P.-F. Piguet, T.W. Mak, and T.R. Ulich. 1996. *Corynebacterium parvum*- and *Mycobacterium bovis* bacillus Calmette-Guérin-induced granuloma formation is inhibited in TNF receptor I (TNF-RI) knockout mice and by treatment with soluble TNF-RI. *J. Immunol.* 157:5022–5026.
22. Marino, M.W., A. Dunn, D. Grail, M. Inglese, Y. Noguchi, E. Richards, A. Jungbluth, H. Wada, M. Moore, B. Williamson, et al. 1997. Characterization of tumor necrosis factor-deficient mice. *Proc. Natl. Acad. Sci. USA.* 94:8093–8098.
23. Tsuji, H., N. Mukaida, A. Harada, S. Kaneko, E. Matsushita, Y. Nakamura, H. Tsutsui, H. Okamura, K. Nakanishi, Y. Tagawa, et al. 1999. Alleviation of lipopolysaccharide-induced acute liver injury in *Propionibacterium acnes*-primed IFN-γ-deficient mice by a concomitant reduction of TNF-α, IL-12, and IL-18 production. *J. Immunol.* 162: 1049–1055.
24. Yoneyama, H., K. Matsuno, Y. Zhang, M. Murai, M. Itakura, S. Ishikawa, G. Hasegawa, M. Naito, H. Asakura, and K. Matsushima. 2001. Regulation by chemokines of circulating dendritic cell precursors and the formation of portal tract–associated lymphoid tissue in a granulomatous liver disease. *J. Exp. Med.* 193:35–49.
25. Sanguedolce, M.V., C. Capo, P. Bongrand, and J.-L. Mege. 1992. Zymosan-stimulated tumor necrosis factor-α production by human monocytes: down-modulation by phorbol ester. *J. Immunol.* 148:2229–2236.
26. Underhill, D.M., A. Ozinsky, A. Hajjar, A. Stevens, C.B. Wilson, M. Bassetti, and A. Aderem. 1999. The Toll-like receptor 2 is recruited to macrophage phagosomes and discriminates between pathogens. *Nature.* 401:811–815.
27. Young, S.-H., J. Ye, D.G. Frazer, X. Shi, and V. Castranova. 2001. Molecular mechanism of tumor necrosis-α production in 1,3-β-glucan (zymosan)-activated macrophages. *J. Biol. Chem.* 276:20781–20787.
28. Daum, T., and M.S. Rohrbach. 1992. Zymosan induces selective release of arachidonic acid from rabbit alveolar macrophages via stimulation of a β-glucan receptor. *FEBS Lett.* 309:119–122.
29. Nobel, P.W., P.M. Henson, C. Lucas, M. Mora-Worms, P.C. Carré, and D.W.H. Riches. 1993. Transforming growth factor-β primes macrophages to express inflammatory gene products in response to particulate stimuli by an autocrine/paracrine mechanism. *J. Immunol.* 151:979–989.

30. Okazaki, M., N. Chiba, Y. Adachi, N. Ohno, and T. Yadomae. 1996. Signal transduction pathway on β-glucans-triggered hydrogen peroxide production by murine peritoneal macrophages in vitro. *Biol. Pharm. Bull.* 19:18–23.
31. Jinnouchi, K., Y. Terasaki, S. Fujiyama, K. Tomita, W.A. Kuziel, N. Maeda, K. Takahashi, and M. Takeya. 2003. Impaired hepatic granuloma formation in mice deficient in C-C chemokine receptor 2. *J. Pathol.* 200:406–416.
32. Yoshimoto, T., K. Nakanishi, S. Hirose, K. Hiroishi, H. Okamura, Y. Takemoto, A. Kanamaru, T. Hada, T. Tamura, E. Kakishita, and K. Higashino. 1992. High serum IL-6 level reflects susceptible status of the host to endotoxin and IL-1/tumor necrosis factor. *J. Immunol.* 148:3596–3603.
33. Gu, Y., K. Kuida, H. Tsutsui, G. Ku, K. Hsiao, M.A. Fleming, N. Hayashi, K. Higashino, H. Okamura, K. Nakanishi, et al. 1997. Activation of interferon-γ inducing factor mediated by interleukin-1β converting enzyme. *Science.* 275:206–209.
34. Merlin, T., A. Sing, P.J. Nielsen, C. Galanos, and M.A. Freudenberg. 2001. Inherited IL-12 unresponsiveness contributes to the high LPS resistance of the LPS (d) C57BL/10ScCr mouse. *J. Immunol.* 166:566–573.
35. Sun, X.M., W. Hsueh, and G. Torre-Amione. 1990. Effects of in vivo "priming" on endotoxin-induced hypotension and tissue injury. The role of PAF and tumor necrosis factor. *Am. J. Pathol.* 136:949–956.
36. Pfeffer, K., T. Matsuyama, T.M. Kündig, A. Wakeham, K. Wiegmann, P.S. Ohashi, M. Krönke, and T.W. Mak. 1993. Mice deficient for the 55 kd tumor necrosis factor receptor are resistant to endotoxic shock, yet succumb to *L. monocytogenes* infection. *Cell.* 73:457–467.
37. Rothe, J., W. Lesslauer, H. Lotscher, Y. Lang, P. Koebel, F. Kontgen, A. Althage, R. Zinkernagel, M. Steinmetz, and H. Bluethmann. 1993. Mice lacking the tumour necrosis factor receptor 1 are resistant to TNF-mediated toxicity but highly susceptible to infection by *Listeria monocytogenes. Nature.* 364:798–802.
38. Car, B.D., V.M. Eng, B. Schnyder, L. Ozmen, S. Huang, P. Galley, D. Heumann, M. Aguet, and B. Ryffel. 1994. Interferon γ receptor–deficient mice are resistant to endotoxic shock. *J. Exp. Med.* 179: 1437–1444.
39. Pasparakis, M., L. Alexopoulou, V. Episkopou, and G. Kollias. 1996. Immune and inflammatory responses in TNFα-deficient mice:a critical requirement for TNFα in the formation of primary B cell follicles, follicular dendritic cell networks and germinal centers, and in the maturation of the humoral immune response. *J. Exp. Med.* 184:1397–1411.
40. Dubois, S.P., T.A. Waldmann, and J.R. Muller. 2005. Survival adjustment of mature dendritic cells by IL-15. *Proc. Natl. Acad. Sci. USA.* 102:8662–8667.
41. Jung, S., D. Unutmaz, P. Wong, G. Sano, K. De los Santos, T. Sparwasser, S. Wu, S. Vuthoori, K. Ko, F. Zavala, et al. 2002. In vivo depletion of $CD11c^+$ dendritic cells abrogates priming of $CD8^+$ T cells by exogenous cell-associated antigens. *Immunity.* 17:211–220.
42. Peterson, J.D., L.A. Herzenberg, K. Vasquez, and C. Waltenbaugh. 1998. Glutathione levels in antigen-presenting cells modulate Th1 versus Th2 response patterns. *Proc. Natl. Acad. Sci. USA.* 95:3071–3076.
43. Murata, Y., M. Amao, J. Yoneda, and J. Hamuro. 2002. Intracellular thiol redox status of macrophages directs the Th1 skewing in thioredoxin transgenic mice during aging. *Mol. Immunol.* 38:747–757.
44. Murata, Y., T. Ohteki, S. Koyasu, and J. Hamuro. 2002. IFN-γ and pro-inflammatory cytokine production by antigen-presenting cells is dictated by intracellular thiol redox status regulated by oxygen tension. *Eur. J. Immunol.* 32:2866–2873.
45. Murata, Y., T. Shimamura, and J. Hamuro. 2002. The polarization of T(h)1/T(h)2 balance is dependent on the intracellular thiol redox status of macrophages due to the distinctive cytokine production. *Int. Immunol.* 14:201–212.
46. Ma, A., R. Koka, and P. Burkett. 2006. Diverse functions of IL-2, IL-5, and IL-7 in lymphoid homeostasis. *Annu. Rev. Immunol.* 24:657–679.
47. Rückert, R., K. Brandt, E. Bulanova, F. Mirghomizadeh, R. Paus, and S. Bulfone-Paus. 2003. Dendritic cell-derived IL-15 controls the induction of CD8 T cell immune responses. *Eur. J. Immunol.* 33:3493–3503.
48. Lodolce, J.P., P.R. Burkett, D.L. Boone, M. Chien, and A. Ma. 2001. T cell–independent interleukin-15α signals are required for bystander proliferation. *J. Exp. Med.* 194:1187–1194.
49. Judge, A.D., X. Zhang, H. Fujii, C.D. Surh, and J. Sprent. 2002. Interleukin-15 controls both proliferation and survival of a subset of memory-phenotype $CD8^+$ T cells. *J. Exp. Med.* 196:935–946.
50. Burkett, P.R., R. Koka, M. Chien, S. Chai, F. Chan, A. Ma, and D.L. Boone. 2003. IL-15Rα expression on $CD8^+$ T cells is dispensable for T cell memory. *Proc. Natl. Acad. Sci. USA.* 100:4724–4729.
51. Burkett, P.R., R. Koka, M. Chien, S. Chai, D.L. Boone, and A. Ma. 2004. Coordinate expression and trans presentation of interleukin (IL)-15Rα and IL-15 supports natural killer cell and memory $CD8^+$ T cell homeostasis. *J. Exp. Med.* 200:825–834.
52. Schluns, K.S., K.D. Klonowski, and L. Lefrancois. 2004. Transregulation of memory CD8 T-cell proliferation by IL-15Rα$^+$ bone marrow-derived cells. *Blood.* 103:988–994.
53. Schluns, K.S., E.C. Nowak, A. Cabrera-Hernandez, L. Puddington, L. Lefrancois, and H.L. Aguila. 2004. Distinct cell types control lymphoid subset development by means of IL-15 and IL-15 receptor α expression. *Proc. Natl. Acad. Sci. USA.* 101:5616–5621.
54. Kuziel, W.A., S.J. Morgan, T.C. Dawson, S. Griffin, O. Smithies, K. Ley, and N. Maeda. 1997. Severe reduction in leukocyte adhesion and monocyte extravasation in mice deficient in CC chemokine receptor 2. *Proc. Natl. Acad. Sci. USA.* 94:12053–12058.
55. Ichiyasu, H., M. Suga, A. Matsukawa, K. Iyonaga, T. Mizobe, T. Takahashi, and M. Ando. 1999. Functional roles of MCP-1 in *Propionibacterium acnes*-induced, T cell-mediated pulmonary granulomatosis in rabbits. *J. Leukoc. Biol.* 65:482–491.
56. Peters, W., H.M. Scott, H.F. Chambers, J.L. Flynn, I.F. Charo, and J.D. Ernst. 2001. Chemokine receptor 2 serves an early and essential role in resistance to *Mycobacterium tuberculosis. Proc. Natl. Acad. Sci. USA.* 98:7958–7963.
57. Kamijo, R., J. Le, D. Shapiro, E.A. Havell, S. Huang, M. Aguet, M. Bosland, and J. Vilcek. 1993. Mice that lack the interferon-γ receptor have profoundly altered responses to infection with Bacillus Calmette-Guerin and subsequent challenge with lipopolysaccharide. *J. Exp. Med.* 178:1435–1440.
58. Sakao, Y., K. Takeda, H. Tsutsui, T. Kaisho, F. Nomura, H. Okamura, K. Nakanishi, and S. Akira. 1999. IL-18-deficient mice are resistant to endotoxin-induced liver injury but highly susceptible to endotoxin shock. *Int. Immunol.* 11:471–480.
59. Hüe, S., J.-J. Mention, R.C. Monteiro, S. Zhang, C. Cellier, J. Schmitz, V. Verkarre, N. Fodil, S. Bahram, N. Cerf-Bensussan, and S.C. Caillat-Zucman. 2004. A direct role for NKG2D/MICA interaction in villous atrophy during celiac disease. *Immunity.* 21:367–377.

Synergistic Pathogenic Effects of Combined Mouse Monoclonal Anti-Desmoglein 3 IgG Antibodies on Pemphigus Vulgaris Blister Formation

Hiroshi Kawasaki[1], Kazuyuki Tsunoda[1,2], Tsuyoshi Hata[1,3], Ken Ishii[1], Taketo Yamada[4] and Masayuki Amagai[1]

Pemphigus vulgaris (PV) is an autoimmune blistering disease caused by anti-desmoglein 3 (Dsg3) IgG antibodies. Previously, we generated an active mouse model for PV by adoptive transfer of splenocytes from immunized or naive $Dsg3^{-/-}$ mice. In this study, we isolated 10 anti-Dsg3 IgG mAbs (NAK-series) from PV model mice generated by transfer of naive $Dsg3^{-/-}$ splenocytes. We characterized their epitopes using domain-swapped and point-mutated Dsg1/Dsg3 molecules and examined their pathogenic activities in blister formation in three different assays. In a passive transfer model using neonatal mice, eight of 10 NAK mAbs showed pathogenic activity when injected together with half the minimum pathogenic dose of anti-Dsg1 IgG autoantibodies from pemphigus foliaceus (PF) patients. None of the mAbs could induce the PV phenotype when individual hybridoma clones were inoculated by peritoneal injection into adult $Rag2^{-/-}$ mice. NAK mAbs displayed a range of potency in an *in vitro* dissociation assay using primary cultured mouse keratinocytes. Interestingly, when multiple hybridoma clones recognizing different epitopes were inoculated in combination, recipient mice developed the PV phenotype. *In vitro* dissociation assays confirmed that combined NAK mAbs had synergistic pathogenic effects. These findings indicate that although an individual anti-Dsg3 IgG is not sufficient to cause blistering in adult mice, several together can induce the PV phenotype. These mAbs will provide a valuable tool to investigate the molecular mechanisms of blister formation, mimicking the effects of the polyclonal IgG antibodies found in patients.

Journal of Investigative Dermatology (2006) **126,** 2621–2630. doi:10.1038/sj.jid.5700450; published online 13 July 2006

INTRODUCTION

Pemphigus vulgaris (PV) is a fatal autoimmune blistering disease of the skin and mucous membranes (Amagai, 2003), which is characterized clinically by flaccid blisters and erosions, and histopathologically by the loss of cell–cell adhesion between basal and suprabasal keratinocytes, resulting in suprabasal acantholysis. The target antigen of PV is desmoglein 3 (Dsg3), a desmosomal transmembrane glycoprotein that belongs to the cadherin gene superfamily of Ca^{2+}-dependent cell–cell adhesion molecules (Amagai *et al.*, 1991; Amagai, 1996). Compelling evidence indicates that IgG autoantibodies against Dsg3 in PV play a primary pathogenic role in blister formation (Anhalt *et al.*, 1982; Amagai *et al.*, 1992, 1998; Mahoney *et al.*, 1999).

Previously, we developed a mouse model for PV using $Dsg3^{-/-}$ mice, which should not acquire immunological tolerance to Dsg3 (Amagai *et al.*, 2000b). After immunization of $Dsg3^{-/-}$ mice with recombinant extracellular domains of mouse Dsg3, we adoptively transferred splenocytes from the immunized mice into $Rag2^{-/-}$ recipient mice that express Dsg3. The transferred $Dsg3^{-/-}$ lymphocytes stably produced anti-Dsg3 IgG and the recipient mice developed a PV phenotype, including oral erosions with histological suprabasilar acantholysis and telogen hair loss (Koch *et al.*, 1997). Subsequently, we demonstrated that the adoptive transfer of naive splenocytes from nonimmunized $Dsg3^{-/-}$ mice to $Rag2^{-/-}$ recipients also induced the production of anti-Dsg3 IgG and the PV phenotype (Aoki-Ota *et al.*, 2004). Antibody production and the appearance of the PV phenotype were delayed by approximately 2 weeks in mice receiving naive splenocytes compared to those receiving immunized splenocytes. However, once the PV phenotype developed, there were no apparent differences in disease severity between mice induced by the two methods. Interestingly, the anti-Dsg3 IgG titers were markedly lower in mice that received naive splenocytes than in mice that received immunized

[1]*Department of Dermatology, Keio University School of Medicine, Shinjuku-ku, Tokyo, Japan;* [2]*Department of Dentistry and Oral Surgery, Keio University School of Medicine, Shinjuku-ku, Tokyo, Japan;* [3]*R&D Division, KOSÉ Corporation, Tokyo, Japan and* [4]*Department of Pathology, Keio University School of Medicine, Shinjuku-ku, Tokyo, Japan*

Correspondence: Dr Masayuki Amagai, Department of Dermatology, Keio University School of Medicine, 35 Shinanomachi, Shinjuku-ku, Tokyo 160-8582, Japan. E-mail: amagai@sc.itc.keio.ac.jp

Abbreviations: Dsg, desmoglein; hDsg, human desmoglein; mDsg, mouse desmoglein; PF, pemphigus foliaceus; PV, pemphigus vulgaris

Received 17 December 2005; revised 19 March 2006; accepted 8 April 2006; published online 13 July 2006

splenocytes, suggesting that the antibodies generated in the former are more potent than those in the latter. Conformational epitope mapping in model mice revealed that anti-Dsg3 IgG were predominantly raised against the middle to C-terminal extracellular domains of mouse Dsg3, where amino-acid residues are less conserved among desmoglein isoforms. PV model mice receiving naive splenocytes produced antibodies against the N-terminal domain of Dsg3 more frequently than mice receiving immunized splenocytes (Anzai *et al.*, 2004).

We isolated eight anti-Dsg3 IgG mAbs from PV model mice that received immunized Dsg3$^{-/-}$ splenocytes (the AK series) (Tsunoda *et al.*, 2003). Two of these mAbs were capable of inducing the loss of cell–cell adhesion in keratinocytes, as determined in a passive transfer model using neonatal mice, and one of the two, AK23, was able to induce the PV phenotype when hybridoma cells were inoculated into the peritoneal cavities of Rag2$^{-/-}$ mice. The other six mAbs failed to show apparent pathogenic activity, in spite of their ability to bind the native Dsg3 *in vivo*.

In the present study, we isolated a further 10 anti-Dsg3 IgG mAbs from PV model mice that received naive Dsg3$^{-/-}$ splenocytes (NAK series). We characterized the pathogenic activities of these mAbs in three different assays (passive transfer, ascites formation, and *in vitro* dissociation), and also analyzed their conformational epitopes. We found that anti-Dsg3 mAbs reacting with different parts of the molecule are synergistic in their pathogenic activity, inducing blister formation when they are combined.

RESULTS

Production of NAK anti-Dsg3 IgG mAbs from PV model mice

As a source of hybridoma cells, we used splenocytes of PV model mice generated by adoptive transfer of splenocytes from naive Dsg3$^{-/-}$ mice, which produce more potent anti-Dsg3 IgG antibodies than mice receiving immunized Dsg3$^{-/-}$ splenocytes (Aoki-Ota *et al.*, 2004). We first screened the hybridoma cells by ELISA against recombinant mouse Dsg3; positive clones were further screened by live staining of mouse keratinocyte PAM212 cells. The second screening selected mAbs that could bind to the native Dsg3 on keratinocyte cell surfaces *in vivo*. Ten independent clones were isolated and designated as NAK mAbs (Table 1).

All of the NAK mAbs had the κ isotype light chain. Four (NAK1, 2, 3, 5) had IgG1 and six (NAK4, 7, 8, 9, 10, 11) had IgG2a heavy chains (Table 1). Under indirect immunofluorescence, all stained keratinocyte cell surfaces in all layers of the mouse oral mucosa, with stronger intensity toward the more basal layers (Figure 1, mouse hard palate and see also Supplementary Figure 1) and in the basal and parabasal layers of the mouse epidermis (Figure 1, mouse tail skin). Five mAbs (NAK1, 4, 7, 8, 9) also stained the keratinocyte cell surfaces of human epidermis, but with different staining patterns. NAK1 and NAK9 mAbs stained the lower layers of the human epidermis, NAK4 stained all layers, and NAK7 and NAK8 stained the middle to upper layers (Figure 1, human epidermis). With ELISA, all of the mAbs reacted only with mouse Dsg3 and not with mouse Dsg1. Those mAbs that showed crossreactivity with human epidermis

Table 1. Characterization of the NAK mAbs

				ELISA								Pathogenic activity		
		IIF[1]		Mouse		Human[2]		Live keratinocyte staining	Ca dependency[3]	Epitopes[4]	Passive transfer[5]	Ascites formation	Dissociation assay[6]
NAK	Isotype	Mouse	Human	Dsg3	Dsg1	Dsg3	Dsg1						
1	IgG1κ	+	+	+	–	+	–	+	+	T25, Y28, Q29	+	–	14.6
2	IgG1κ	+	–	+	–	–	–	+	+	195–402	+	–	25.2
3	IgG1κ	+	–	+	–	+	–	+	–	403–565	–	–	0.5
4	IgG2aκ	+	+	+	–	+	+	+	+	1–162	+	–	35.9
5	IgG1κ	+	–	+	–	–	–	+	–	195–402	–	–	12.5
7	IgG2aκ	+	+	+	–	–	+	+	+	1–162	+	–	13.4
8	IgG2aκ	+	+	+	–	–	+	+	+	1–162	+	–	25.4
9	IgG2aκ	+	+	+	–	+	–	+	+	T25, Y28, Q29, V53 D54, K55, N56	+	–	45.1
10	IgG2aκ	+	–	+	–	–	–	+	+	1–162	+	–	34.9
11	IgG2aκ	+	–	+	–	–	–	+	+	1–402	+	–	33.6

IIF, indirect immunofluorescence.
[1]Indirect immunofluorescence staining. Mouse oral mucosa (hard palate) and human normal skin were used as the substrates.
[2]ELISA reactivity against human Dsgs was determined with 0.1 μg/ml NAK mAbs.
[3]The reactivity of NAK mAbs against mouse Dsg3 was determined with or without EDTA treatment. +, indicates the abolition of the reactivity by EDTA.
[4]The epitopes are indicated by the residue numbers for mouse Dsg3 except those for NAK1 and NAK9 mAbs, whose epitopes are indicated by the residues for human Dsg3.
[5]+, indicates gross blister formation when coinjected with PF IgG.
[6]Dissociation index values are listed when dissociation index obtained by AK23 mAb (Tsunoda *et al.*, 2003) is 100.

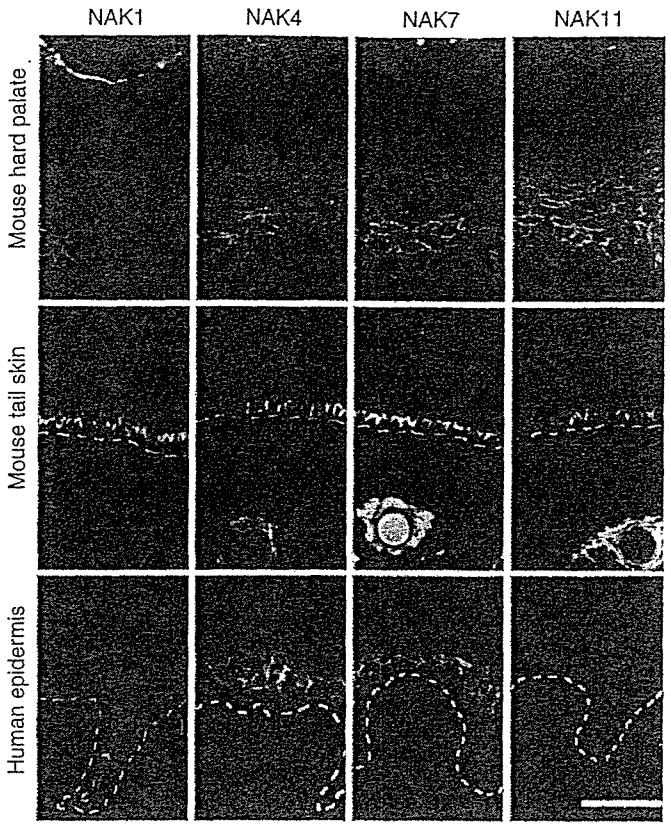

Figure 1. Immunostaining of mouse and human tissues with NAK mAbs. Representative immunostaining is shown (NAK1, NAK4, NAK7, and NAK11). All of the NAK mAbs stained keratinocyte cell surfaces in all layers of mouse oral mucosa (mouse hard palate), with stronger intensity toward the lower layers, and stained the lower layers of mouse epidermis (mouse tail skin), where Dsg3 is expressed. NAK mAbs reacted with human epidermis in different patterns (human epidermis); NAK1, NAK4, and NAK7 mAbs stained the lower portion of, the entire, and the upper portion of human epidermis, respectively, while NAK11 failed to react with human epidermis. Dashed lines indicate the basement membrane zone. Bar = 50 μm.

under immunofluorescence also recognized human Dsg3 and/or Dsg1 in different patterns. NAK1, NAK3, and NAK9 reacted with human Dsg3, NAK4 reacted with both human Dsg3 and Dsg1, and NAK7 and NAK8 reacted with human Dsg1 (Table 1). The immunofluorescence staining patterns of NAK mAbs whose IIF was positive on human epidermis (NAK1, 4, 7, 8, 9) were consistent with the ELISA results, based on the distribution of Dsg1 and Dsg3 in the human epidermis (Amagai *et al.*, 1996; Shirakata *et al.*, 1998).

Thus, all NAK mAbs specifically reacted with native mouse Dsg3 without crossreacting with mouse Dsg1, and some crossreacted with human Dsg3 and/or Dsg1 in different patterns.

NAK mAbs recognize different epitopes on Dsg3

To characterize the epitopes of the NAK mAbs, we determined whether their binding to mouse Dsg3 was dependent on calcium. Treating a mouse Dsg3-coated ELISA plate with EDTA did not substantially alter binding of NAK3 and NAK5, but abolished binding of the other mAbs (data not shown). Therefore, NAK3 and NAK5 mAbs recognized Ca^{2+}-independent epitopes, while the other mAbs recognized Ca^{2+}-dependent conformational epitopes.

To map the epitopes of the mAbs, we used domain-swapped mouse Dsg3/Dsg1 recombinant molecules (Anzai *et al.*, 2004). These molecules are believed to maintain native conformations, at least in terms of binding anti-Dsg IgG antibodies (Futei *et al.*, 2000; Sekiguchi *et al.*, 2001). We used four domain-swapped molecules that contained the mouse Dsg3 residues 1–162 ($mDsg3^{1-162}/mDsg1^{163-512}$), 1–402 ($mDsg3^{1-402}/mDsg1^{403-512}$), 195–565 ($mDsg1^{1-194}/mDsg3^{195-565}$), or 403–565 ($mDsg1^{1-402}/mDsg3^{403-565}$). NAK1, 4, 7, 8, 9, 10 mAbs precipitated residues 1–162 and 1–402, but not residues 195–565 or 403–565 (Figure 2a and b). Their epitopes appear to reside in residues 1–162, the N-terminal portion of the extracellular domain of mouse Dsg3. NAK2 and NAK5 reacted with residues 1–402 and 195–565, but not with residues 1–162 or 403–565 (Figure 2a and b). Their epitopes appear to be in residues 195–402, which represent the middle portion of the extracellular domain. NAK3 precipitated residues 195–565 and 403–565, but not residues 1–162 or 1–402 (Figure 2a and b). Its epitope appears to reside in residues 403–565, the C-terminal portion of the extracellular domain. NAK11 mAb precipitated only residues 1–402 (Figure 2a and b).

Of these mAbs, NAK1 and NAK9 crossreacted with human Dsg3 but not with human Dsg1, and recognized the N-terminal residues 1–162. We used a series of point-mutated human Dsg3 and Dsg1 molecules, in which Dsg3-specific residues were replaced by the corresponding Dsg1-specific residues, or *vice versa* (Figure 2d; Tsunoda *et al.*, 2003). NAK1 mAb maintained its reaction with human Dsg3 mutated at T31, K33, I34 (Dsg3-M2), V53-N56 (Dsg3-M3), E70, S73 (Dsg3-M4), L75, T77 (Dsg3-M5), A83, and Q84 (Dsg3-M6), but lost reactivity when the Dsg3 specific residues T25, Y28, or Q29 were mutated (Dsg3-M1, M1-2, M1-2-3) (Figure 2c and d). NAK1 gained recognition of human Dsg1 modified with Dsg3-specific residues at T25, Y28, or Q29 (Dsg1-M1-2, M1-2-3) (Figure 2c and d). These findings indicate that the epitope for NAK1 maps to the T25, Y28, and Q29 of Dsg3. T25 and Q29 are conserved between human and mouse Dsg3, but Y28 in the human is replaced by F28 in the mouse.

Similarly, NAK9 mAb reacted with human Dsg3 mutated at Dsg3-specific residues T31, K33, I34 (Dsg3-M2), E70, S73 (Dsg3-M4), L75, T77 (Dsg3-M5), A83, and Q84 (Dsg3-M6), but lost recognition when either T25, Y28, Q29 (M1), or V53-N56 (Dsg3-M3) were mutated (Figure 2c and d). NAK9 gained recognition of human Dsg1 when mouse residues T25, Y28, Q29, and V53-N56 were introduced (Dsg1-M1-2-3), but not when T25, Y28, and Q29 were introduced with T31, K33, and I34 (Dsg1-M1-2) (Figure 2c and d). These findings indicate that the epitope of NAK9 mAb maps to the residues T25, Y28, Q29, V53, D54, K55, and N56. Of these, Y28 and K55 are not conserved in mouse Dsg3 (F28, P55).

Thus, these NAK mAbs recognize different epitopes on Dsg3, and six of them recognize the N-terminal 1–162 residues (Table 1).

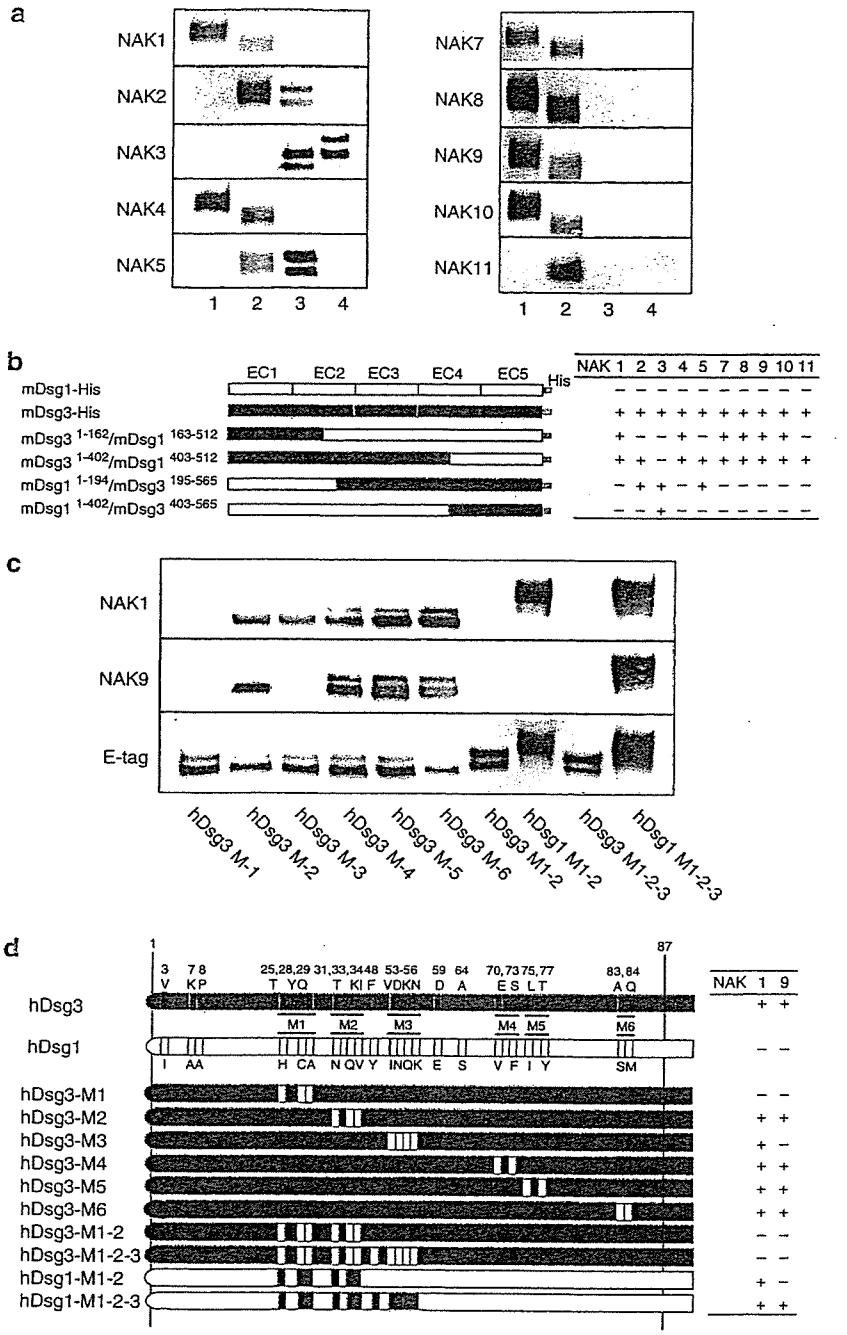

Figure 2. Immunoprecipitation of domain-swapped and point-mutated Dsg1/Dsg3 recombinant proteins with NAK mAbs. (a) Immunoprecipitation of mDsg3$^{1-162}$/mDsg1$^{163-512}$ (lane 1), mDsg3$^{1-402}$/mDsg1$^{403-512}$ (lane 2), mDsg1$^{1-194}$/mDsg3$^{195-596}$ (lane 3), and mDsg1$^{1-402}$/mDsg3$^{403-565}$ (lane 4) with various NAK mAbs. (b) The molecular structure of domain-swapped mDsg1/mDsg3 proteins and summary of results for epitope mapping of mAbs. (c) Immunoprecipitation of various point-mutated hDsg1/hDsg3 proteins with NAK1 (upper panel), NAK9 (middle panel), and anti-E-tag mAb as a positive control (lower panel). (d) The molecular structure of point-mutated hDsg1/hDsg3 proteins and summary of results for epitope mapping of NAK1 and NAK9 mAbs. The 22 amino-acid residues not conserved between hDsg1 and hDsg3 are indicated. These nonconserved residues were switched between Dsg1 and Dsg3 to generate point-mutated molecules.

Most NAK mAbs induce blisters in passive transfer to neonatal mice

To evaluate the pathogenic activities of the mAbs, we first performed a passive transfer assay using neonatal mice, a well-established assay for pemphigus (Anhalt *et al.*, 1982; Amagai *et al.*, 1994). Purified IgG from the culture supernatant of each hybridoma was injected s.c. into neonatal mice, and the mice were observed for 18–24 hours postinjection (Table 2). When individual NAK mAbs were injected, none of them induced gross blistering; this was expected, as

Dsg1 co-expression in the skin of neonatal mice compensates for the impaired adhesive function of Dsg3 (Figure 3; Amagai, 1999; Mahoney *et al.*, 1999). However, all of the mAbs except NAK3 induced varying degrees of microscopic blistering, with histological evidence of suprabasilar acantholysis (Figure 3). We scored the extent of this blistering using the total area of blisters observed in histology (Table 2).

To overcome the compensation by Dsg1, we used IgG prepared from pemphigus foliaceus (PF) sera that contained anti-Dsg1 IgG autoantibodies. We injected one-half of the minimum dose of PF IgG that had been shown to induce gross blisters, alone or in combination with NAK mAbs (Tsunoda *et al.*, 2003). Neonatal mice that were co-injected with each of the NAK mAbs (except NAK3 and NAK5) developed extensive gross blisters with suprabasilar acantholysis, while mice injected with the PF IgG alone did not show any blister formation (Figure 3).

These findings indicate that most of the NAK mAbs are able to induce the loss of cell–cell adhesion of keratinocytes in neonatal mice. Only two failed to show pathogenic effects.

Table 2. Summary of the pathogenic activities of NAK mAbs in passive transfer assay

	NAK alone[1]			NAK+PF IgG[2]	
			Blister formation		
NAK	*n*	IgG deposition	Histologic blister Scores[3]	*n*	Gross blisters
1	3	+	5.70	3	3
2	3	+	16.31	2	2
3	3	+	0	2	0
4	3	+	38.91	3	1
5	3	+	4.04	2	0
7	3	+	4.82	2	2
8	3	+	6.38	2	2
9	3	+	22.23	2	2
10	3	+	4.77	4	2
11	3	+	9.48	2	2

PF, pemphigus foliaceus.
[1]NAK mAbs alone were subcutaneously injected into neonatal mice and the formation of gross or microscopic blisters was noted.
[2]NAK mAbs were coinjected with 50% of the minimum dose of PF IgG into neonatal mice and the formation of gross blisters was noted. The number of mice with the gross blisters was listed.
[3]The blister score is defined in Materials and Methods.

None of the individual NAK mAbs induce the PV phenotype in adult mice

To further evaluate the pathogenic activities of NAK mAbs, we inoculated individual hybridoma cells intraperitonealy into $Rag2^{-/-}$ immunodeficient mice (6–8 weeks old), and looked for the appearance of the PV phenotype, which includes weight loss, patchy hair loss, and mucosal erosions (Figure 4, Table 3). None of the recipient mice developed this phenotype, even after obvious ascites fluid formation at day 15. Although all the mice showed *in vivo* IgG deposition on keratinocyte cell surfaces of the skin and mucous membranes, no blister formation was apparent in the oral mucosa at the histological level (Figure 4).

These findings indicate that none of the individual NAK clones inoculated was potent enough to induce the loss of cell–cell adhesion of keratinocytes *in vivo*, during ascites formation in adult mice.

Combined NAK mAbs induce the PV phenotype in adult mice

To explore the possibility of combined pathogenic effects, we inoculated NAK hybridoma cells intraperitonealy in various combinations into $Rag2^{-/-}$ mice (Figure 4, Table 3). When hybridoma cells for NAK1, 2, 4, 7, 8, 9, 10, and 11 were combined, the recipient mice developed weight loss, patchy hair loss, and crusted erosions around the snout, at approximately days 10–15 after the inoculation. These mice showed suprabasilar acantholysis of the oral mucosa and in the skin around the snout, together with *in vivo* IgG deposition on keratinocyte surfaces. The titers of circulating anti-Dsg3 IgG in the recipient mice with combined NAK hybridoma cells were compatible with those with single NAK hybridoma cells. The development of the PV phenotype was observed even after mAbs NAK8, NAK4, NAK10, and NAK9 were sequentially removed from the combination (Table 3). The minimum combination that was sufficient to induce the PV phenotype in all recipient mice tested was NAK1, NAK2, NAK7, and NAK11, or NAK2, NAK3, NAK5, and NAK11,

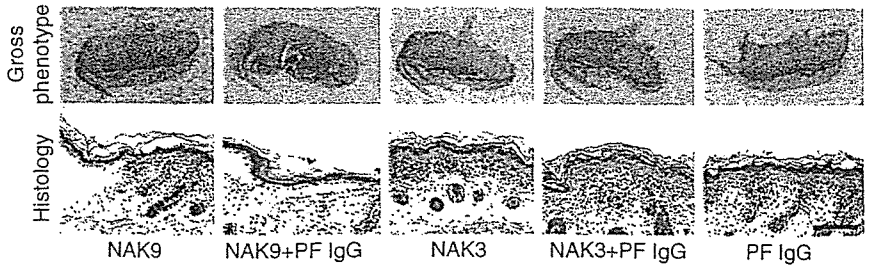

Figure 3. Passive transfer assay of NAK mAbs in neonatal mice. All antibodies except NAK3 and NAK5 mAbs (which recognize Ca^{2+}-independent epitopes) induced gross PV blisters when co-injected with a dose of PF IgG insufficient to induce blisters on its own. Representative data are shown. Neonatal mice injected with NAK9, but not with NAK3, developed microscopic blisters with histological suprabasilar acantholysis, without apparent gross blisters. Neonatal mice co-injected with NAK9, but not NAK3 or PF IgG alone, developed extensive blistering (arrows) with suprabasilar acantholysis. Bar = 50 μm.

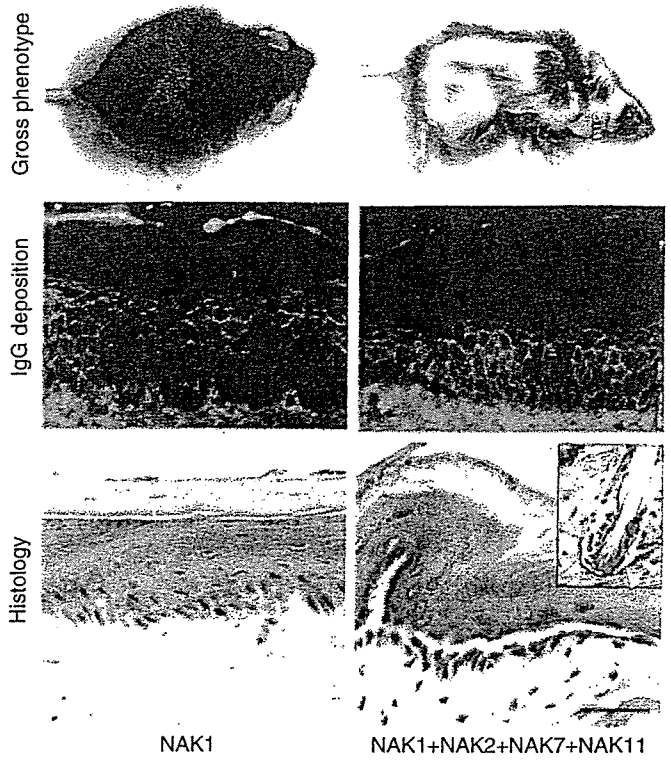

Figure 4. Combinations of NAK mAbs induced the PV phenotype when their hybridoma cells were inoculated intraperitonealy, while the individual mAbs failed to do so. Mice inoculated with NAK1 hybridoma cells alone did not develop apparent PV phenotype (day 15 after inoculation) or histological suprabasilar acantholysis, in spite of apparent ascites formation and *in vivo* IgG deposition on keratinocyte cell surfaces of stratified squamous epithelia. In contrast, when hybridoma cells producing NAK1, NAK2, NAK7, and NAK11 mAbs were combined, recipient mice developed patchy hair loss as well as weight loss (day 15). Histology of the oral mucosa showed *in vivo* IgG deposition and suprabasilar acantholysis and the skin showed acantholysis around telogen hair club (inset; arrow heads indicate the location of acantholysis). Bar = 50 μm.

each of which recognize different epitopes on mouse Dsg3 (Table 1). The mice inoculated with hybridoma cells from these clones developed the full spectrum of PV phenotypic markers (Figure 4).

When we removed any NAK hybridoma cells from the above minimum combination, some of the recipient mice started not to develop the PV phenotype and the other mice showed the PV phenotype at approximately days 15–20 after the inoculation (Table 3). The minimum combination that could induced the PV phenotype at least one of the mice tested was NAK2 and NAK11 hybridoma cells (Table 3).

These findings indicate that NAK mAbs that are not sufficient to induce blisters singly are capable of doing so in adult mice when they are combined.

Pathogenic ranking of NAK mAbs by *in vitro* dissociation assay

The passive transfer assay with neonatal mice and the ascites formation assay with $Rag2^{-/-}$ adult mice require relatively large amounts of antibodies, and do not necessarily simulate pathogenesis in a quantitative fashion. We recently developed an *in vitro* dissociation assay using primary cultures of normal human keratinocytes, as a simple method to quantify the pathogenic strength of pemphigus autoantibodies (Ishii *et al.*, 2005). For this study, we modified the assay to evaluate the pathogenic activity of NAK mAbs against mouse keratinocytes. To obtain Dsg3-dominated cell–cell adhesion, we used primary cultured mouse keratinocytes, which express a low level of Dsg2, in the presence of exfoliative toxin A, which specifically digests Dsg1 (Amagai *et al.*, 2000a). After incubation with various NAK mAbs, a sheet of keratinocytes, released by dispase, were subjected to mechanical stress by pipetting, and the number of cell sheet fragments was determined. The number of cell fragments

Table 3. Summary of the pathogenic activities of NAK mAbs in ascites formation assays

NAK	*n*	IgG deposition[1]	PV phenotype[2] (*n* (%))	Titers of circulating anti-Dsg3 IgG[3]
1	7	+	0	144.2±9.3
2	4	+	0	72.9±1.3
3	10	+	0	230.6±38.9
4	5	+	0	ND
5	11	+	0	181.0±20.0
7	3	+	0	92.0±1.0
8	4	+	0	85.3±1.3
9	8	+	0	111.6±4.2
10	8	+	0	41.1±3.3
11	6	+	0	ND
1,2,4,7,8,9,10,11	5	+	5 (100)	114.0±14.7
1,2,4,7,9,10,11	3	+	3 (100)	113.6±0.1
1,2,7,9,11	2	+	2 (100)	ND
1,2,7,11	7	+	7 (100)	126.5±5.9
2,3,5,11	3	+	3 (100)	219.3±5.9
2,7,11	3	+	2 (67)	77.2±6.7
1,2,11	4	+	2 (50)	112.1±2.8
1,2,7	4	+	0	218.3±5.9
1,7,11	4	+	0	175.5±13.0
2,3,5	3	+	0	208.8±5.9
2,11	3	+	1 (33)	55.7±5.6
2,7	2	+	0	94.1±21.5
7,11	3	+	0	ND

ND, not determinded; PV, pemphigus vulgaris.
Hybridoma cells for individual NAK clones or combinations were inoculated intraperitonealy into $Rag2^{-/-}$ mice.
[1]IgG deposition on mouse keratinocyte cell surfaces was observed in all mice injected with NAK mAb hybridomas.
[2]The development of the PV phenotype, including patchy hair loss and suprabasilar acantholysis of the oral mucosa, was evaluated. The number of mice with the PV phenotype was listed.
[3]Titers of circulating anti-Dsg3 IgG were measured by mDsg3 ELISA at days 15–20 days after inoculation.

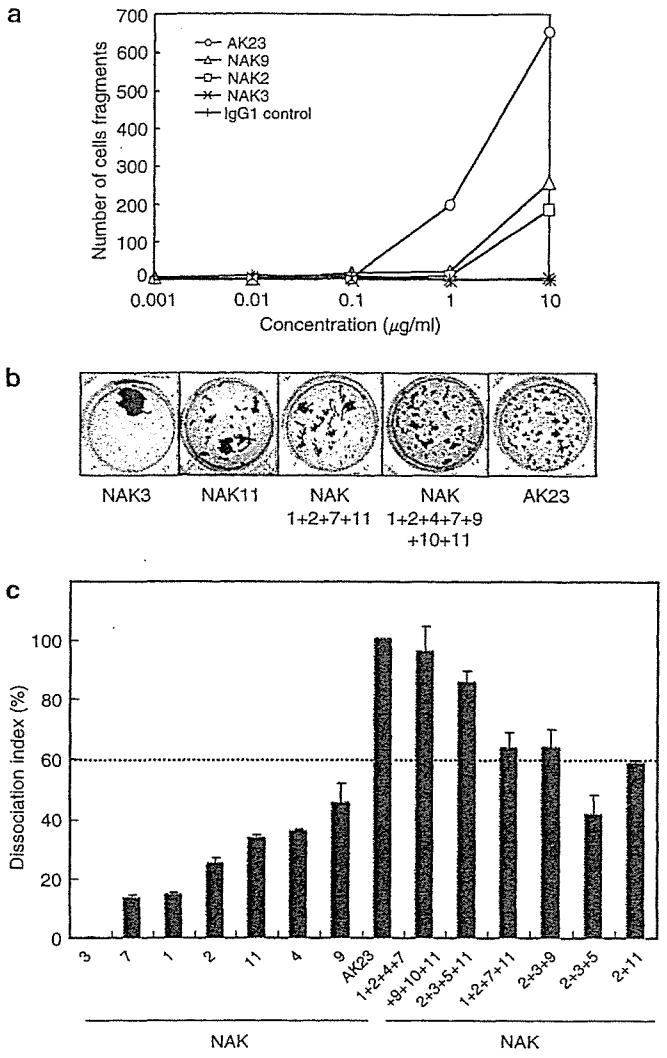

Figure 5. *In vitro* keratinocyte dissociation assays demonstrated synergistic pathogenic effects of NAK mAbs in the loss of keratinocyte cell–cell adhesion. Sheets of mouse keratinocytes were treated with exfoliative toxin A to digest Dsg1and with NAK mAbs, and subjected to mechanical stress. Cell fragments were counted by image analysis. Representative data are shown. (**a**) Dose dependency of NAK mAbs on dissociation scores. (**b**) NAK11 induced fragmentation while NAK3 did not. The combined mAbs generated similar numbers of cell fragments as did AK23, an anti-Dsg3 mAb that is able to induce the PV phenotype (Tsunoda *et al.*, 2003). (**c**) Dissociation indexes of NAK mAbs alone and in combination. The dissociation index varied among the mAbs. Combinations of mAbs (adjusted to 1 μg/ml) had higher dissociation indexes than individual NAK mAbs. Combining these data with the results from ascites formation assays indicates that the threshold for blister formation *in vivo* may be at a dissociation index of approximately 60% (dashed line).

increased as the concentration of AK23 or various NAK mAbs increased, indicating that this assay evaluate pathogenic strength in a quantitative manner (Figure 5a). Dissociation index values were calculated as a percent of the number of fragments obtained with a positive control mAb, AK23 (Tsunoda *et al.*, 2003).

Each NAK mAb had a different dissociation index, indicating that this assay could discriminate differences in activity among them (Table 1, representative data are shown in Figure 5b and c). NAK3 and NAK5, which failed to induce apparent pathogenic activity in the passive transfer model, gave smaller dissociation indexes than the others (0.5 and 12.5%, respectively), while NAK9 had the highest dissociation index (45.1%).

When several NAK mAbs were combined, without changing the total amount of IgG added (1 μg/ml), dissociation scores greatly increased (Figure 5c). When NAK1, 2, 4, 7, 9, 10, and 11 mAbs were combined, the dissociation score was equivalent to that of the AK23 mAb, hybridoma cells of which can alone induce the PV phenotype in adult mice (Tsunoda *et al.*, 2003). When we removed some of NAK mAbs from the combination, the dissociation scores gradually decreased in general. The dissociation scores of the all combinations were still higher than those of the individual NAK mAbs, indicating a synergistic pathogenic effect (representative data in Figure 5c). Considering these results with those of the ascites formation assay, we speculate that there may be a threshold of blister formation *in vivo* in adult mice corresponding to a dissociation index of approximately 60% (dashed line in Figure 5c).

These findings indicate that individual NAK mAbs have various pathogenic activities in disrupting the cell–cell adhesion mediated by Dsg3, none individually potent enough to induce an apparent PV phenotype in adult mice. However, combinations of these mAbs show synergistic effects above the threshold for blister formation and development of the PV phenotype.

DISCUSSION

In this study, we generated 10 anti-Dsg3 IgG mAbs from PV model mice produced by adoptive transfer of naive Dsg3$^{-/-}$ splenocytes. All mAbs specifically reacted with native mouse Dsg3, but not with mouse Dsg1. Some (NAK1, 3, 4, 7, 8, 9) cross-reacted with human Dsgs, although the isoform specificities of the mAbs were not necessarily conserved between mouse and human. NAK1, NAK3, and NAK9 reacted only with human Dsg3, while NAK4 reacted with both human Dsg3 and Dsg1, and NAK7 and NAK8 reacted only with human Dsg1. These findings indicate that antibodies against Dsgs have fine specificities, determined by the few amino-acid residues that are not conserved between mouse and human isoforms. This highlights the difficulty of performing detailed evaluations of these mouse antibodies using human skin or keratinocytes and *vice versa*.

We performed three different assays to evaluate the pathogenic activities of NAK mAbs: passive transfer, ascites formation, and *in vitro* dissociation. The passive transfer assay, by injection of IgG into neonatal mice, is well established (Anhalt *et al.*, 1982), and the ascites formation assay, after inoculation of hybridoma cells into immunodeficient adult mice, has been developed to evaluate *in vivo* pathogenic activity of anti-Dsg3 mAbs (Tsunoda *et al.*, 2003). The passive transfer assay is more easily controlled than the ascites formation assay. Highly concentrated IgG can be applied to neonatal mice by passive transfer, while the